

Self-consistent thermodynamic description of silicate liquids, with application to shock melting of MgO periclase and MgSiO₃ perovskite

Nico de Koker^{1*} and Lars Stixrude^{1,2}

¹Department of Geological Sciences, University of Michigan, Ann Arbor, Michigan, USA. E-mail: nico.dekoker@uni-bayreuth.de

²Department of Earth Sciences, University College London, UK

Accepted 2009 February 4. Received 2009 February 4; in original form 2008 October 2

SUMMARY

We develop a self-consistent thermodynamic description of silicate liquids applicable across the entire mantle pressure and temperature regime. The description combines the finite strain free energy expansion with an account of the temperature dependence of liquid properties into a single fundamental relation, while honouring the expected limiting behaviour at large volume and high temperature. We find that the fundamental relation describes well previous experimental and theoretical results for liquid MgO, MgSiO₃, Mg₂SiO₄ and SiO₂. We apply the description to calculate melting curves and Hugoniot of solid and liquid MgO and MgSiO₃. For periclase, we find a melting temperature at the core–mantle boundary (CMB) of 7810 ± 160 K, with the solid Hugoniot crossing the melting curve at 375 GPa, 9580 K, and the liquid Hugoniot crossing at 470 GPa, 9870 K. For complete shock melting of periclase we predict a density increase of 0.14 g cm⁻³ and a sound speed decrease of 2.2 km s⁻¹. For perovskite, we find a melting temperature at the CMB of 5100 ± 100 K with the perovskite section of the enstatite Hugoniot crossing the melting curve at 150 GPa, 5190 K, and the liquid Hugoniot crossing at 220 GPa, 5520 K. For complete shock melting of perovskite along the enstatite principal Hugoniot, we predict a density increase of 0.10 g cm⁻³, with a sound speed decrease of 2.6 km s⁻¹.

Key words: Mantle processes; Equations of state; High-pressure behaviour; Phase transitions; Planetary interiors; Physics of magma and magma bodies.

1 INTRODUCTION

Liquid state thermodynamics have long played a central role in the study of mantle petrology and geochemistry. The chemical history of a terrestrial planet is intimately tied to its thermal history through fractionation processes associated with cooling of a magma ocean and melting of a solid mantle (Ohtani & Sawamoto 1987; Ohtani 1988; Miller *et al.* 1991b; Agee & Walker 1993; Solomatov & Stevenson 1993). Furthermore, seismic observations suggest the presence of partial melt atop the 410 km discontinuity (Revenaugh & Sipkin 1994; Song *et al.* 1994) and at the base of the mantle (Garnero & Helmberger 1995; Williams & Garnero 1996; Revenaugh & Meyer 1997). Accurate estimates of the solidus temperature of the mantle at those depths can thus provide key constraints on the composition and geothermal profile of the mantle. Decompression melting close to the free surface is responsible for the mafic and ultramafic igneous rocks that, together with mantle xenoliths, provide our most direct chemical observations of the

Earth's deep interior. Accurate estimates of the equations of state and phase equilibria of melts constrain the pressures at which melting primarily occurs (McKenzie & Bickle 1988; Asimow *et al.* 1995) and the depth limits from which melts can reach the surface (Stolper *et al.* 1981; Agee & Walker 1988, 1993; Rigden *et al.* 1989; De Koker *et al.* 2008).

While the equations of state of many solid mantle phases have been measured to lower mantle pressures (Stixrude & Lithgow-Bertelloni 2005, and references therein), the experimental study of silicate liquids remains challenging, even at low pressures (Lange & Carmichael 1987; Rigden *et al.* 1989; Lange & Navrotsky 1992; Shen & Lazor 1995; Ai & Lange 2008). First principles molecular dynamics (FPMD) studies (Trave *et al.* 2002; Laudernet *et al.* 2004; Stixrude & Karki 2005; Karki *et al.* 2006, 2007; Wan *et al.* 2007; De Koker *et al.* 2008; Sun 2008) have recently focused on silicate liquids at pressures and temperatures relevant to the full extent of the Earth's mantle, and revealed rich structural and thermodynamic compressional behaviour. Thermodynamic properties were found to be significantly different from those of solids: the isochoric heat capacity (C_V) is generally larger than the high temperature limit seen in solids ($3Nk_B$) and varies significantly on compression; the Grüneisen parameter (γ) increases with compression,

*Now at: Bayerisches Geoinstitut, University of Bayreuth, Germany.

whereas it always decreases during isostructural compression of solids.

In this study, we develop a self-consistent thermodynamic description of liquid state thermodynamics relevant to silicate liquids at pressures and temperatures characteristic of mantles and magma oceans associated with terrestrial planets. We apply our thermodynamic formalism to the description of FPMD results, using these as a guide to the functional forms and the relevant physics. In addition, we derive an anharmonic fundamental relation for solids at high temperature (i.e. in the classical limit), which we combine with the liquid descriptions to obtain melting curves and theoretical Hugoniot loci for MgO periclase and MgSiO₃ perovskite.

2 PREVIOUS WORK

PVT equations of state were first described for the ideal gas (Boyle 1662; Clapeyron 1834). This equation of state treats particles as independent, and is thus unable to describe the liquid–vapour transition. At high pressures, this relation is commonly applied to stellar interiors (Chandrasekhar 1939; Phillips 1994), but it does not capture the comparative incompressibility of terrestrial materials such as silicate liquids at the conditions characteristic of planetary interiors. Subsequent Van der Waals (van der Waals 1873) and Redlich–Kwong (Redlich & Kwong 1949) equations were formulated to capture critical behaviour and the liquid–vapour transition, but are only valid close to ambient conditions, predicting very incompressible behaviour at higher pressure. Modified Redlich–Kwong forms (Halbach & Chatterjee 1982; Holland & Powell 1991; Brodholt & Wood 1993) address this problem, but require many free parameters to constrain. Similarly, other empirical and semi-empirical forms, developed primarily for interpolation of large data sets of liquid and gas thermodynamic properties (Belonoshko & Saxena 1992; Pitzer & Sterner 1994; Span & Wagner 1997), also require large numbers of free parameters with consequent poor extrapolation and unphysical oscillations in thermodynamic properties. None of these existing forms are thus able to capture the essentials of silicate liquids over a geophysically interesting pressure range with sufficiently few free parameters.

The Thomas–Fermi model (Slater & Krutter 1935; Marshak & Bethe 1940; Feynman *et al.* 1949) gives an approximate description of the equation of state at very high pressures, based on a simplified model of the electronic charge density. It has been successfully applied to stellar and gas giant interiors, but is too approximate to offer insight into the behaviour of materials within the Earth’s interior (Birch 1952; Knopoff & Uffen 1954). In high pressure hydrodynamic simulations these problems are remedied to some extent by the quotidian equation of state (More *et al.* 1988; Young & Corey 1995), which, however, makes a number of simplifying assumptions, in particular the Dulong–Petit law and the Lindemann law, that have been shown not to hold for silicate melts (Stebbins *et al.* 1984; Wolf & Jeanloz 1984; Stixrude & Karki 2005; Karki *et al.* 2007; De Koker *et al.* 2008).

Experimental studies of the equation of state of silicate liquids have been almost entirely limited to ambient and uppermost mantle pressures (Bottinga 1985; Lange & Carmichael 1987; Agee & Walker 1988, 1993; Courtial *et al.* 1997; Lange 1997; Ai & Lange 2008), with only a few shock loading and multi-anvil measurements giving insight into the equation of state at pressures characteristic of the lower mantle (Rigden *et al.* 1984, 1989; Miller *et al.* 1991a; Chen *et al.* 2002; Suzuki & Ohtani 2003; Matsukage *et al.* 2005; Sakamaki *et al.* 2006; Mosenfelder *et al.* 2007, 2009). These re-

sults have shown that simple polynomial descriptions of $P(V, T)$ or $V(P, T)$ (Ghiorso & Sack 1995) are inadequate at high pressure (Ghiorso 2004). The Birch–Murnaghan equation of state (Birch 1952, 1978) has been widely used (Rigden *et al.* 1989; Ghiorso *et al.* 2002; Lange 2003; Suzuki & Ohtani 2003; Matsukage *et al.* 2005; Sakamaki *et al.* 2006; Lange 2007), but more high pressure data are needed to test its validity. While the Birch–Murnaghan equation of state and similar forms, such as the Universal equation of state, have been widely and successfully tested against measurements on solids (Jeanloz 1989; Anderson 1995; Cohen *et al.* 2000), this has not been done for silicate liquids. Indeed, the suitability of the Birch–Murnaghan form has been questioned on a theoretical basis (Hofmeister 1993; Ghiorso 2004).

A key issue which has not been carefully addressed, is the thermal contribution to the liquid equation of state. In describing the temperature and pressure dependence of a material simultaneously, great care must be taken to preserve thermodynamic self-consistency (Dorogokupets 2000; Ghiorso *et al.* 2002; Pavese 2002; Ghiorso 2004; Ai & Lange 2008). The main goal of the work presented here is to derive a thermodynamic treatment of silicate liquids which self-consistently describes their thermal and compressional behaviour.

3 FUNDAMENTAL THERMODYNAMIC RELATIONS

The basis of our approach is an expression for the Helmholtz free energy

$$F = F(V, T), \quad (1)$$

as a function of its natural variables, volume (V) and temperature (T). We follow Callen (1985) in referring to $F(V, T)$ as a ‘fundamental thermodynamic relation’, because all thermodynamic information may be self-consistently obtained from it by differentiation, reduction of derivatives and Legendre transformations,

$$P = - \left(\frac{\partial F}{\partial V} \right)_T, \quad (2)$$

$$S = - \left(\frac{\partial F}{\partial T} \right)_V, \quad (3)$$

$$K_T = V \left(\frac{\partial^2 F}{\partial V^2} \right)_T, \quad (4)$$

$$\alpha K_T = - \left(\frac{\partial^2 F}{\partial V \partial T} \right), \quad (5)$$

$$C_V = -T \left(\frac{\partial^2 F}{\partial T^2} \right)_V, \quad (6)$$

$$\frac{\gamma}{V} = \frac{\alpha K_T}{C_V}, \quad (7)$$

$$\frac{K_S}{K_T} = \frac{C_P}{C_V} = (1 + T\alpha\gamma), \quad (8)$$

$$G = F - V \left(\frac{\partial F}{\partial V} \right)_T = F + PV, \quad (9)$$

$$E = F - T \left(\frac{\partial F}{\partial T} \right)_V = F + TS, \quad (10)$$

$$H = F - T \left(\frac{\partial F}{\partial T} \right)_V - V \left(\frac{\partial F}{\partial V} \right)_T = F + TS + PV. \quad (11)$$

By deriving all the equilibrium thermodynamics from a single function, self-consistency among properties is guaranteed through Maxwell relations.

3.1 Liquids

The fundamental thermodynamic relation of the liquid phase is

$$F(V, T) = F_{\text{ig}}(V, T) + F_{\text{xs}}(V, T) + F_{\text{el}}(V, T), \quad (12)$$

where we have assumed the three contributions to F to be separable (McQuarrie 1984). These contributions are: an ideal gas term (F_{ig}) arising from momenta of the atoms, an excess term (F_{xs}) which accounts for interatomic interaction, and an electronic term (F_{el}) describing the free energy due to thermal excitation of electrons.

3.1.1 Atomic momentum contribution

The atomic momentum contribution (ideal gas term) is given by an ideal mixture of the ideal gas free energy ($F_{\text{ig}M}$) for the respective types of atoms (M) that make up the liquid (Lupis 1983; McQuarrie 1984),

$$F_{\text{ig}} = \sum_M N_M F_{\text{ig}M} + k_B N_A T \sum_M N_M \ln X_M, \quad (13)$$

$$F_{\text{ig}M} = -k_B N_A T \left[\ln V_M + \frac{3}{2} \ln T + \frac{3}{2} \ln \left(\frac{m_M k_B}{2\pi\hbar^2} \right) + 1 \right], \quad (14)$$

where

$$X_M = \frac{N_M}{\sum_M N_M}, \quad (15)$$

N_A is Avogadro's number, k_B is the Boltzmann constant, m_M and V_M is, respectively, the mass and unit volume of one particle of type M and N_M is the number of atoms of each type per formula unit.

3.1.2 Excess contribution

Let $f = f(V)$ and $\theta = \theta(T)$ such that $f(V_0) = 0$ and $\theta(T_0) = 0$, with V_0 and T_0 the reference volume and temperature. Expand F_{xs} in f and θ about the origin in a 2-D Taylor series. From the resulting excess free energy

$$F_{\text{xs}}(V, T) = \sum_{i=0}^{\mathcal{O}_f'} \sum_{j=0}^{\mathcal{O}_\theta'} \frac{a_{ij}}{i!j!} f^i \theta^j, \quad (16)$$

follows

$$P_{\text{xs}}(V, T) = -\frac{\partial f}{\partial V} \sum_{i=0}^{\mathcal{O}_f'} \sum_{j=0}^{\mathcal{O}_\theta'} \frac{i a_{ij}}{i!j!} f^{i-1} \theta^j, \quad (17)$$

$$S_{\text{xs}}(V, T) = -\frac{\partial \theta}{\partial T} \sum_{i=0}^{\mathcal{O}_f'} \sum_{j=0}^{\mathcal{O}_\theta'} \frac{j a_{ij}}{i!j!} f^i \theta^{j-1}, \quad (18)$$

$$E_{\text{xs}}(V, T) = \sum_{i=0}^{\mathcal{O}_f'} \sum_{j=0}^{\mathcal{O}_\theta'} \frac{a_{ij}}{i!j!} f^i \theta^{j-1} \left(\theta - j T \frac{\partial \theta}{\partial T} \right), \quad (19)$$

$$K_{T_{\text{xs}}}(V, T) = V \sum_{i=0}^{\mathcal{O}_f'} \sum_{j=0}^{\mathcal{O}_\theta'} \frac{i a_{ij}}{i!j!} \theta^j \times \left[\left(\frac{\partial^2 f}{\partial V^2} \right) f^{i-1} + \left(\frac{\partial f}{\partial V} \right)^2 (i-1) f^{i-2} \right], \quad (20)$$

$$(\alpha K_T)_{\text{xs}}(V, T) = -\left(\frac{\partial f}{\partial V} \right) \left(\frac{\partial \theta}{\partial T} \right) \sum_{i=0}^{\mathcal{O}_f'} \sum_{j=0}^{\mathcal{O}_\theta'} \frac{i j a_{ij}}{i!j!} f^{i-1} \theta^{j-1}, \quad (21)$$

$$C_{V_{\text{xs}}}(V, T) = -T \sum_{i=0}^{\mathcal{O}_f'} \sum_{j=0}^{\mathcal{O}_\theta'} \frac{j a_{ij}}{i!j!} f^i \times \left[\left(\frac{\partial^2 \theta}{\partial T^2} \right) \theta^{j-1} + \left(\frac{\partial \theta}{\partial T} \right)^2 (j-1) \theta^{j-2} \right], \quad (22)$$

where we denote the respective orders of expansion in f and θ as \mathcal{O}_f and \mathcal{O}_θ , and primes on sums indicate that $i + j < \mathcal{O}_f + \mathcal{O}_\theta$ must be satisfied.

We follow Birch (1952, 1978) and choose

$$f = \frac{1}{n} \left[\left(\frac{V_0}{V} \right)^{\frac{n}{3}} - 1 \right], \quad (23)$$

which reduces to the Eulerian finite strain for $n = 2$. For $T = T_0$, eq. (17) reduces to the Birch–Murnaghan equation of state.

By also describing the thermal variable θ as

$$\theta = \left[\left(\frac{T}{T_0} \right)^m - 1 \right], \quad (24)$$

the internal energy (eq. 19) becomes

$$E_{\text{xs}}(V, T) = \sum_{i=0}^{\mathcal{O}_f} \sum_{j=0}^{\mathcal{O}_\theta} \frac{a_{ij}}{i!j!n} \left[\left(\frac{V_0}{V} \right)^{\frac{n}{3}} - 1 \right]^i \left[\left(\frac{T}{T_0} \right)^m - 1 \right]^{j-1} \times \left[\left(\frac{T}{T_0} \right)^m (1 - jm) - 1 \right], \quad (25)$$

which, after applying the binomial theorem and rearranging terms can be expressed along a given isochore V as a polynomial function of T^m

$$E_{\text{xs}}(V, T) = \sum_{j=0}^{\mathcal{O}_\theta} b_j(V) \left(\frac{T}{T_0} \right)^{jm}, \quad (26)$$

where

$$b_j(V) = \sum_{i=0}^{\mathcal{O}_f} \sum_{k=1}^{\infty} (-1)^k a_{i(j+k-1)} \frac{(jm-1)}{(n(i)!(j)!(k-1)!)} \times \left[\left(\frac{V_0}{V} \right)^{\frac{n}{3}} - 1 \right]^i. \quad (27)$$

3.1.3 Thermal electronic contribution

Our simulations, as well as shock wave experiments (Hicks *et al.* 2006), show significant electronic contributions to the equation of state. However, the form of the electronic terms differ from those familiar in the case of solid metals. Whereas in metals, the electronic heat capacity increases linearly in temperature from zero Kelvin, in silicate liquids the electronic contributions become significant only above a large, finite temperature T_{el} . The value of T_{el} appears to be

related to melting, although, for generality, we will not assume that T_{el} is identical to the melting temperature here. We therefore adopt the form for the electronic heat capacity

$$C_{V\text{el}}(V, T) = \begin{cases} \zeta(V)[T - T_{\text{el}}(V)] & T \geq T_{\text{el}} \\ 0 & T < T_{\text{el}} \end{cases}, \quad (28)$$

where ζ is the thermo-electronic heat capacity coefficient and depends only on volume.

With electronic entropy (S_{el}) and free energy (F_{el}) zero at $T \leq T_{\text{el}}$, integration yields

$$S_{\text{el}} = \zeta \left[T - T_{\text{el}} - T_{\text{el}} \ln \frac{T}{T_{\text{el}}} \right], \quad (29)$$

$$F_{\text{el}} = -\zeta \left[\frac{1}{2} (T^2 - T_{\text{el}}^2) - T T_{\text{el}} \ln \frac{T}{T_{\text{el}}} \right], \quad (30)$$

from which the electronic energy (E_{el}) and pressure (P_{el}) follow as

$$E_{\text{el}} = \frac{1}{2} \zeta [T - T_{\text{el}}]^2, \quad (31)$$

$$P_{\text{el}} = \frac{\partial \zeta}{\partial V} \left[\frac{1}{2} (T^2 - T_{\text{el}}^2) - T T_{\text{el}} \ln \frac{T}{T_{\text{el}}} \right] + \zeta \frac{\partial T_{\text{el}}}{\partial V} \left[(T - T_{\text{el}}) - T \ln \frac{T}{T_{\text{el}}} \right]. \quad (32)$$

We will describe the volume dependence of ζ and T_{el} with a power-law relation (Bukowinski 1977)

$$\zeta = \zeta_0 \left(\frac{V}{V_0} \right)^\xi, \quad (33)$$

$$T_{\text{el}} = T_{\text{el}0} \left(\frac{V}{V_0} \right)^\eta. \quad (34)$$

3.1.4 Limiting behaviour

The liquid relation is designed such that the infinite temperature and volume limits capture the expected material properties at those conditions, given suitable values of n and m . Limiting values of the excess properties, derived from eqs (17)–(22) are summarized in Table 1. Total values follow from addition of ideal gas, excess and thermo-electronic terms, with the exception of the Grüneisen parameter which is not additive.

Furthermore, the non-electronic portion of the liquid relation captures the physics of the liquid–vapour transition at moderately high volumes, although the power-law parametrization of volume dependence in the thermo-electronic contribution does not capture the limiting behaviour of F_{el} as $V \rightarrow \infty$.

Table 1. Theoretical behaviour of excess thermodynamic properties in the limit of an ideal gas, and values of n and m such that these limits hold. $C(T)$ denotes a limiting value which depends only on T .

	$\lim_{V \rightarrow \infty}$	n	$\lim_{T \rightarrow \infty}$	m
P_{xs}	0	> -3	∞	> 0
S_{xs}	$C(T)$	> 0	0	$< 1/\mathcal{O}_\theta$
E_{xs}	$C(T)$	> 0	∞	> 0
$K_{T\text{xs}}$	0	$> -3/2$	∞	> 0
$\alpha K_{T\text{xs}}$	0	> -3	0	$< 1/\mathcal{O}_\theta$
$C_{V\text{xs}}$	$C(T)$	> 0	0	$< 1/\mathcal{O}_\theta$

3.2 Solids at high temperature

We follow previous studies (Stixrude & Bukowinski 1990a; Stixrude & Lithgow-Bertelloni 2005) and describe the solid by

$$F(V, T) = F(V_0, T_0) + F_{\text{cmp}}(V, T_0) + F_{\text{th}}(V, T), \quad (35)$$

with the assumption that the various contributions to F are separable. $F(V_0, T_0)$ is the free energy at reference volume (V_0) and temperature (T_0), $F_{\text{cmp}}(V, T_0)$ and $F_{\text{th}}(V, T)$ are the compressional and thermal contributions to the free energy, respectively. The contribution due to atomic momentum (F_{ig}) is negligible, and the thermo-electronic contribution (F_{el}) is negligible for iron-free oxides and silicate minerals.

F_{cmp} is expressed as an expansion in terms of the Eulerian finite strain (f) (Birch 1952, 1978)

$$F_{\text{cmp}} = 9K_{T_0}V_0 \left[\frac{1}{2}f^2 + \frac{1}{6}a_3f^3 + \frac{1}{24}a_4f^4 + \dots \right], \quad (36)$$

$$a_3 = 3(K'_{T_0} - 4), \quad (37)$$

$$a_4 = 9[K_{T_0}K''_{T_0} + K'_{T_0}(K'_{T_0} - 7)] + 143, \quad (38)$$

$$f = \frac{1}{2} \left[\left(\frac{V_0}{V} \right)^{\frac{2}{3}} - 1 \right]. \quad (39)$$

The familiar form of the Birch–Murnaghan equation of state follows as the isothermal volume derivative of eq. (36). V_0 , K_{T_0} , K'_{T_0} and K''_{T_0} are the volume, bulk modulus, and its first and second pressure derivatives at zero pressure and a reference temperature (T_0).

F_{th} is obtained by integration of the entropy

$$F_{\text{th}} = - \int_{T_0}^T S(V, T') dT', \quad (40)$$

with the entropy in turn following from integration of the relevant second-order properties

$$S(V, T) = S(V_0, T_0) + \int_{V_0}^V \frac{C_V \gamma(V', T_0)}{V'} dV' + \int_{T_0}^T \frac{C_V(V, T')}{T'} dT'. \quad (41)$$

C_V is taken as constant, although its value is not constrained to allow for anharmonicity, so that F_{th} now follows as

$$F_{\text{th}}(V, T) = -S_0(T - T_0) - C_V \left[T \ln \frac{T}{T_0} - (T - T_0) \right] - C_V(T - T_0) \int_{V_0}^V \frac{\gamma(V', T_0)}{V'} dV'. \quad (42)$$

Applying eqs (2), (3) and (10) to eq. (35), we have

$$E(V, T) = E_0 + 9K_{T_0}V_0 \left[\frac{1}{2}f^2 + \frac{1}{6}a_3f^3 + \frac{a_4}{24}f^4 + \dots \right] + C_V[T - T_0] + C_V[T - T_0] \int_{V_0}^V \frac{\gamma(V', T_0)}{V'} dV', \quad (43)$$

$$P(V, T) = 3K_{T_0}(1 + 2f)^{\frac{5}{2}} \left[f + \frac{a_3}{2}f^2 + \frac{a_4}{6}f^3 + \dots \right] + C_V[T - T_0] \frac{\gamma(V, T_0)}{V}. \quad (44)$$

Through the Maxwell relation

$$\frac{1}{T} \left(\frac{\partial C_V}{\partial V} \right)_T = \frac{1}{V} \left(\frac{\partial C_V \gamma}{\partial T} \right)_V, \quad (45)$$

C_V independent of V and T implies that γ is independent of T . We consider two possible forms to describe $\gamma(V)$. Our preferred form is that of Stixrude & Lithgow-Bertelloni (2005)

$$\gamma = \frac{\gamma'_0 + (2\gamma'_0 + \gamma'_1)f + 2\gamma'_1 f^2}{6(1 + \gamma'_0 f + \gamma'_1 f^2)}, \quad (46)$$

with

$$\gamma_0 = \frac{1}{6}\gamma'_0, \quad (47)$$

and

$$q_0 = \frac{\gamma'_1 + 2\gamma'_0 - 6\gamma_0'^2}{-3\gamma_0'}, \quad (48)$$

which they showed to be superior to the second form we consider, the power law form extensively applied in the literature

$$\gamma = \gamma_0 \left(\frac{V}{V_0} \right)^{q_0}, \quad (49)$$

where γ_0 and q_0 are constants.

4 FIRST PRINCIPLES MOLECULAR DYNAMICS SIMULATIONS

To test the solid and liquid fundamental relations, we use FPMD simulation results for MgO periclase, MgSiO₃ perovskite (Stixrude & Karki 2005), as well as liquid MgO (Karki *et al.* 2006), MgSiO₃ (Stixrude & Karki 2005), Mg₂SiO₄ (De Koker *et al.* 2008) and SiO₂ (Karki *et al.* 2007). With the application to shock melting in mind, we supplement the MgSiO₃ and MgO liquid data of Stixrude & Karki (2005) and Karki *et al.* (2006) at high pressures. These systems are melted at higher temperatures (8000 and 15 000 K, respectively), and then cooled isochorically as in previous calculations. Mg₂SiO₄ and MgSiO₃ liquid simulations at 2000 K are also added to improve constraints at ambient pressure. We therefore have simulations spanning a range of compression of $V/V_X = 0.35$ –1.20, where V_X is an experimental estimate of the liquid volume at ambient conditions.

Our computational technique is described in detail in our previous work, and we only highlight a few salient points here. FPMD simulations based on Density Functional Theory (DFT, Hohenberg & Kohn 1964; Kohn & Sham 1965) are performed as implemented in the VASP plane-wave code (Kresse & Furthmüller 1996), using pseudo-potentials (Kresse & Hafner 1994), the local density approximation (LDA, Ceperley & Alder 1980) and a single k -point at the Brillouin zone centre (Γ). Systems consist of 64 (MgO liquid and periclase), 112 (Mg₂SiO₄ liquid), 80 (MgSiO₃ liquid and perovskite) and 72 atoms (SiO₂ liquid) in a periodic simulation cell. The cell is cubic for liquid simulations, with solid cell dimensions adjusted to obtain a hydrostatic stress tensor. Simulations are performed in the canonical ensemble (constant NVT) through the use of a thermostat (Nosé 1984). We use a time increment of 1.0 fs and run durations of at least 3000 fs, sufficient for converged values of the pressure and internal energy, the mean values of which are obtained using the blocking method (Flyvberg & Petersen 1989).

Computational efficiency is significantly increased by the use of a small basis set, for which the energy is converged but a correction to the pressure (P_{Pulay}) is required (Gomes Dacosta *et al.* 1986; Francis & Payne 1990; De Koker *et al.* 2008). A further correction P_{emp} for the overbinding of the LDA is applied to the pressure (Karki *et al.* 2001; Oganov *et al.* 2001), for which thermodynamic self-consistency requires an adjustment to the energy of

$$E_{\text{emp}}(V) = -P_{\text{emp}}[V - V_0], \quad (50)$$

where V_0 is the zero-pressure volume and we have defined $E_{\text{emp}}(V_0) = 0$.

Because atomic motion in molecular dynamics simulations is entirely classical at all temperatures (Allen & Tildesley 1987; Frenkel & Smit 1996), energy values do not capture the quantum effects characteristic of atomic vibrations at low temperature in solids, and are thus only physical in the limit of high temperatures. Quantum corrections can be applied (Wigner 1932; Kirkwood 1933; Matsui 1989), but our interest here is in solids close to melting where such corrections will be negligible.

The electronic entropy is obtained from the electronic eigenvalues (ϵ_i) as (Mermin 1965; Kresse & Furthmüller 1996)

$$S_{\text{el}}^{\text{DFT}} = -2k_B \sum_i [\phi(\epsilon_i) \ln \phi(\epsilon_i) + [1 - \phi(\epsilon_i)] \ln [1 - \phi(\epsilon_i)]], \quad (51)$$

where $\phi(\epsilon_i)$ is the Fermi–Dirac distribution function

$$\phi(\epsilon_i) = \frac{1}{e^{\beta(\epsilon_i - \epsilon_f)} + 1}, \quad (52)$$

with $\beta = 1/k_B T$. The Fermi energy (ϵ_f) is determined by the number criterion.

5 DETERMINATION OF PARAMETERS

To constrain the liquid relation, electronic entropy is fit to eq. (29), with the subsequent E_{el} and P_{el} , together with the relevant E_{ig} and P_{ig} values, removed from the total E and P values to obtain E_{xs} and P_{xs} . That is

$$E_{\text{xs}} = E_{\text{MD}} - E_{\text{el}} - E_{\text{ig}}, \quad (53)$$

$$P_{\text{xs}} = P_{\text{MD}} - P_{\text{el}} - P_{\text{ig}}. \quad (54)$$

These excess values are then fit to eqs (19) and (17) in a single least squares inversion to constrain coefficients a_{ij} , which in turn are related to physical properties at the reference pressure (P_0) and temperature (T_0) (eqs A5–A19). The free parameters which describe the solid— E_0 , C_V , γ_0 , q_0 , K_0 , K'_0 —are similarly determined by inversion of the total E and P from FPMD to eqs (43) and (44).

To complete the constraints on the fundamental relation, either the free energy or the entropy must be known at a single reference point, which fixes the value of a_{00} (eq. 16). This remaining parameter affects only the absolute values of the thermodynamic potentials, and thus phase equilibria, such as the melting curve, but not other thermodynamic properties, which do not depend on the value of a_{00} (eqs 17–22). As absolute values of the free energy or entropy are very costly to compute via molecular dynamics simulations, our approach in this study is to obtain the entropy of the liquid by matching Gibbs free energies at one point on the melting curve (P_m , T_m)

$$H_{\text{MD}}^{\text{l}}(P_m, T_m) - T_m S_0^{\text{l}}(P_m, T_m) = H_{\text{MD}}^{\text{s}}(P_m, T_m) - T_m S_X^{\text{s}}(P_m, T_m), \quad (55)$$

where superscripts s and l refer to solid and liquid phases respectively, and S_X^{s} is the entropy of the solid computed via the experimentally based thermodynamic model of Stixrude & Lithgow-Bertelloni (2005). Our approach is in principle equivalent to integrating the Clausius–Clapeyron equation from P_m , T_m (Stixrude & Karki 2005; De Koker *et al.* 2008), but is numerically more precise, as the integration is performed analytically. The reference melting point for MgO periclase is taken to be $T_m = 3070$ K, $P_m = 0$ GPa (Riley

1966; Dubrovinsky & Saxena 1997; Alfe 2005). It has been suggested that B4, rather than B1 may be the liquidus phase of MgO at pressures less than 10 GPa (Aguado & Madden 2005), in which case the proper reference temperature would be that of metastable B1 melting at a temperature somewhat less than 3070 K. However, the difference is likely to be small (<200 K, Aguado & Madden 2005). We follow Stixrude & Karki (2005) and use $T_m = 2900$ K, $P_m = 25$ GPa as reference melting temperature for MgSiO₃ perovskite. Note that because the solid equation of state that we have used here is only valid above the Debye temperature, we have chosen in all cases values of the reference temperature that exceed the Debye temperature.

The reference internal energy (E_r) of polymorphs stable at ambient pressure and temperature, needed for calculating the Hugoniot are found as the sum of the static (E_{st}), zero point (E_{zp}) and thermal (E_{th}) contributions to the internal energy

$$E_r(V_r, 300 \text{ K}) = E_{st}(V_r) + E_{zp}(V_r, 0 \text{ K}) + E_{th}(V_r, 300 \text{ K}), \quad (56)$$

where V_r is the experimental volume at 0 GPa, 300 K. We find E_{st} via fully converged static DFT calculations of MgSiO₃ *Pbca* orthoenstatite and MgO periclase. The remaining terms are computed via the experimentally based thermodynamic model of Stixrude & Lithgow-Bertelloni (2005) with the explicit expression for E_{zp} in the Debye–Grüneisen approximation given, for example, in Panero & Stixrude (2004).

To perform the fit for the liquid, the order to which the excess free energy needs to be expanded must be determined and n and m specified. Considering its overwhelming success in fitting and extrapolating high pressure equations of state, we adopt the Eulerian finite strain in our description for melts as well, that is, we use $n = 2$. Similarly, the correct limiting behaviour as $T \rightarrow \infty$ requires $m < 1$ for $\mathcal{O}_\theta = 1$ and $m < 1/2$ for $\mathcal{O}_\theta = 2$. A unique value of m is determined for each composition within the constraints required by the value of \mathcal{O}_θ required to fit the data.

6 RESULTS

6.1 Liquids

Consistent with the conclusions in the original studies, we find that MgO, Mg₂SiO₄ and MgSiO₃ liquid equations of state are sufficiently described with a third-order finite strain expansion ($\mathcal{O}_f = 3$), while SiO₂ requires a fifth-order expansion ($\mathcal{O}_f = 5$) (Figs 1–4). Values of m that optimize the first ($\mathcal{O}_\theta = 1$) and second ($\mathcal{O}_\theta = 2$) order fits to the FPMD data, are noted in Table 2. Our preferred models are those where our FPMD results can be accurately represented with the smallest number of free parameters. $\mathcal{O}_\theta = 1$ yields accurate fits for MgO, Mg₂SiO₄ and MgSiO₃ (Figs 1–3), but is insufficient for SiO₂ (Fig. 4) where high temperature low density points are poorly modelled. These discrepancies are remedied

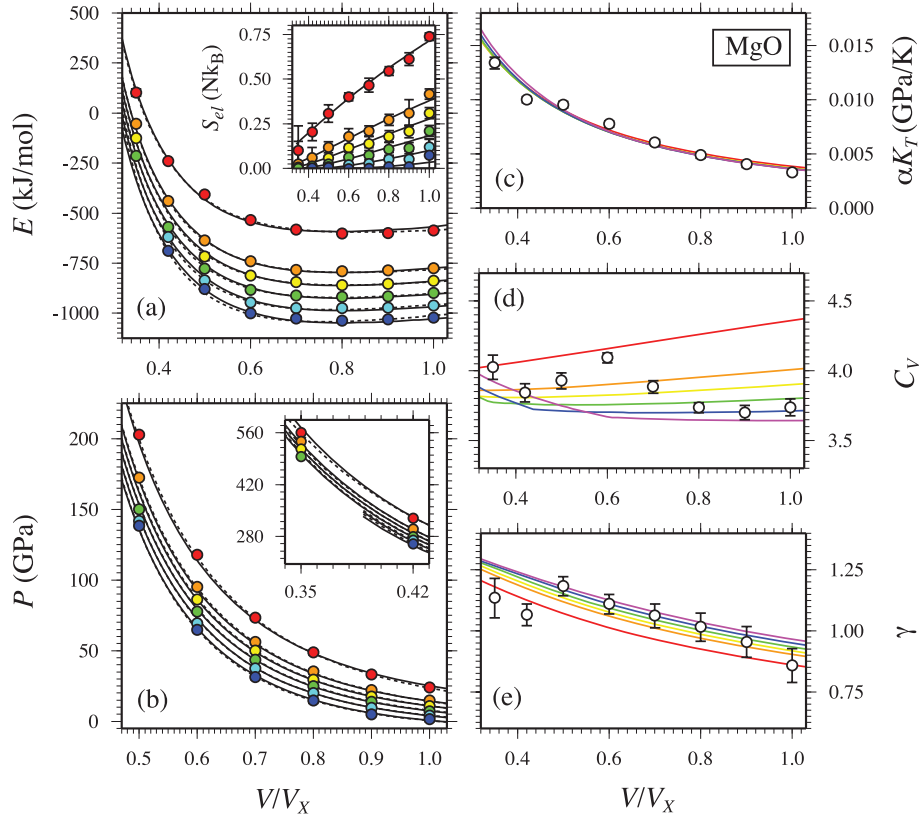


Figure 1. (a) Internal energy (E), (a, inset) thermal electronic entropy (S_{el}), (b) Pressure (P), (c) thermal pressure coefficient (αK_T), (d) isochoric heat capacity (C_V) and (e) Grüneisen parameter (γ) of MgO liquid. Coloured circles in (a) and (b) show values from FPMD simulations at 3000 K (blue), 4000 K (cyan), 5000 K (green), 6000 K (yellow), 7000 K (orange) and 10000 K (red) (Karki *et al.* 2006, except for points at $V/V_X = 0.35$ and $V/V_X = 0.42$). Black lines indicate the fit of P and E to eq. (16) with $\mathcal{O}_\theta = 1$ (solid lines; first order in T , see text) and $\mathcal{O}_\theta = 2$ (dashed lines; second order in T , see text), and a third-order expansion in finite strain. Errorbars are smaller than the size of the symbols. Black lines in (a, inset) indicates the fit to eq. (30). Lines in (c), (d) and (e) are second derivatives of the fundamental relation, coloured by temperatures as the symbols in (a) and (b). These lines follow the trend previously found (Karki *et al.* 2006) by independent linear fits of FPMD results along each simulated isochore (white symbols), but it should be kept in mind that these points represent mean values over a large temperature range, which is not thermodynamically self-consistent, and may also be off due to the glass transition.

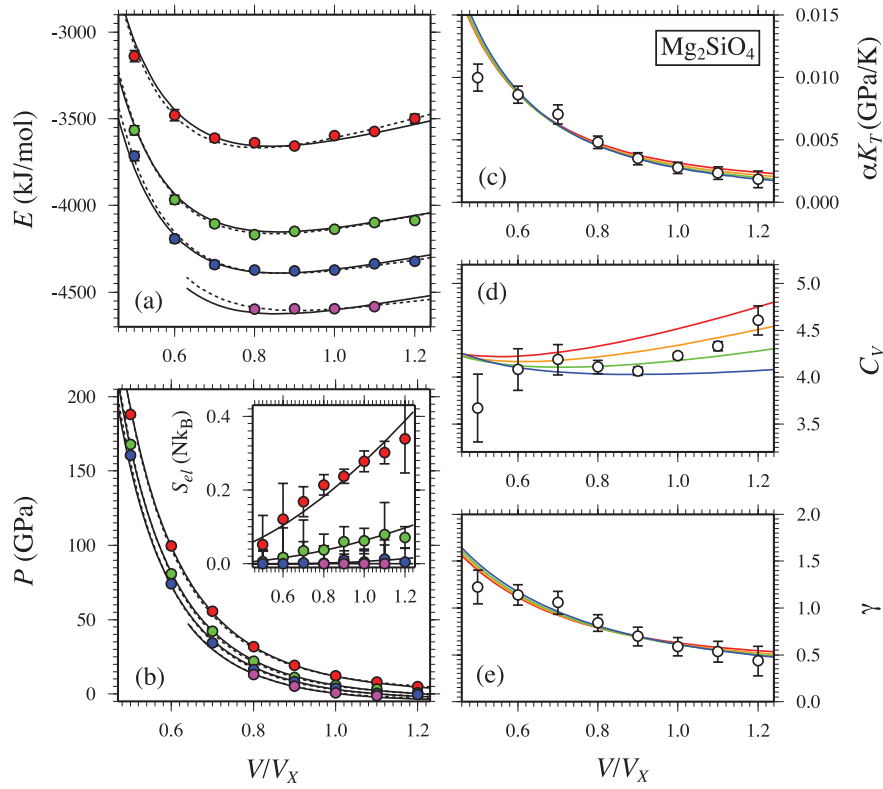


Figure 2. Same as Fig. 1, but for Mg_2SiO_4 liquid. Coloured circles in (a) and (b) show values from FPMD simulations at 2000 K (purple), 3000 K (blue), 4000 K (green) and 6000 K (red) (De Koker *et al.* 2008, except for points at 2000 K). Black lines indicate the fit of P and E to eq. (16) with $\mathcal{O}_\theta = 1$ (solid lines) and $\mathcal{O}_\theta = 2$ (dashed lines), and a third-order expansion in finite strain. White symbols in (c), (d) and (e) are the mean values from (De Koker *et al.* 2008).

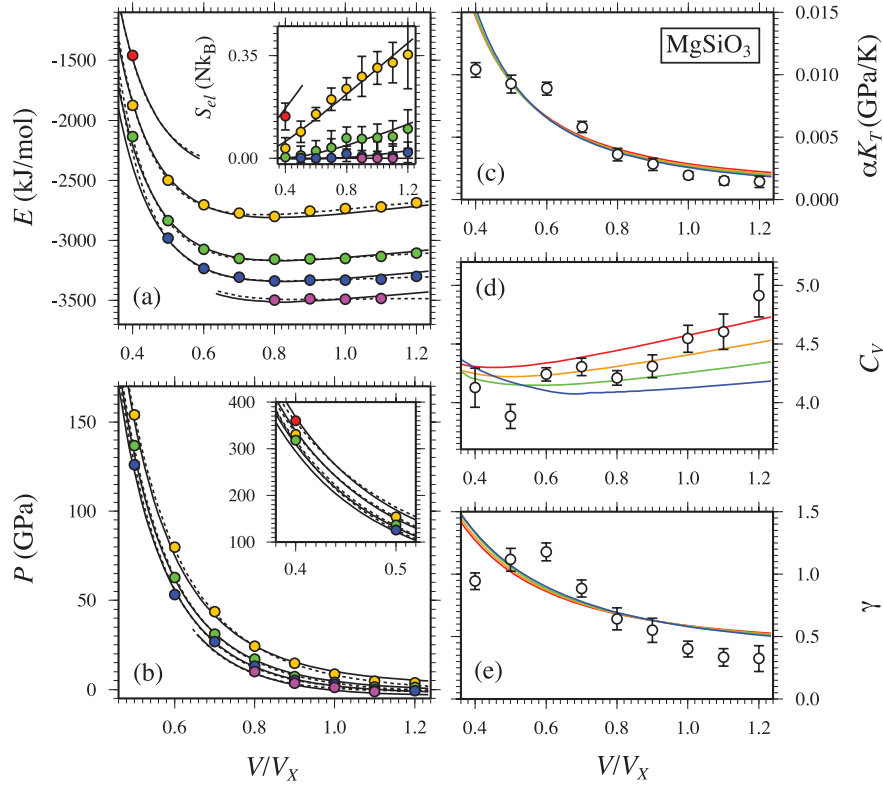


Figure 3. Same as Fig. 2, but for MgSiO_3 liquid. Coloured circles in (a) and (b) show values from FPMD simulations at 2000 K (purple), 3000 K (blue), 4000 K (green), 6000 K (yellow) and 8000 K (red) (Stixrude & Karki 2005, except for points at 2000 K and at $V/V_x = 0.4$). Black lines indicate the fit of P and E to eq. 16 with $\mathcal{O}_\theta = 1$ (solid lines) and $\mathcal{O}_\theta = 2$ (dashed lines), and a third-order expansion in finite strain. White symbols in (c), (d) and (e) are the mean values from (Stixrude & Karki 2005).

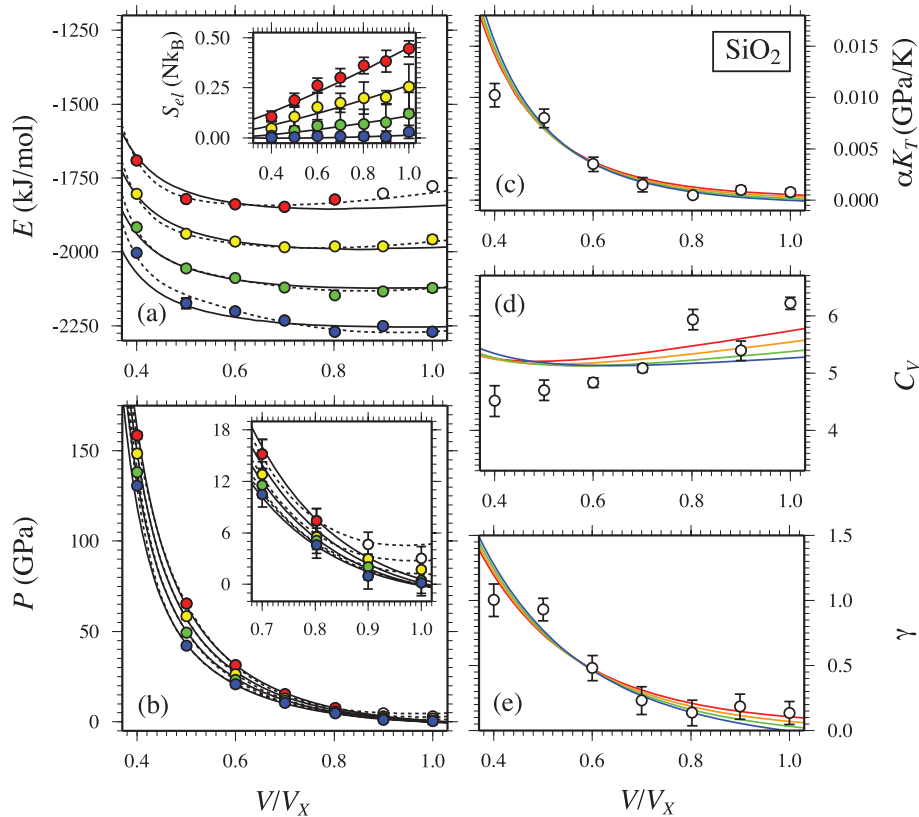


Figure 4. Same as Fig. 3, but for SiO_2 liquid. Coloured circles in (a) and (b) show values from FPMD simulations at 3000 K (blue), 4000 K (green), 5000 K (yellow) and 6000 K (red, white) (Karki *et al.* 2007). Black lines indicate the fit of P and E to eq. (16) with $\mathcal{O}_\theta = 1$ (solid lines) and $\mathcal{O}_\theta = 2$ (dashed lines), and a fifth-order expansion in finite strain. Lines in (c), (d) and (e) are second derivatives of the $\mathcal{O}_\theta = 1$ fundamental relation. White symbols in (c), (d) and (e) are the mean values from, and may be off due to the glass transition (Karki *et al.* 2007).

Table 2. m values used in liquids F_{xs} fits.

\mathcal{O}_θ	MgO	Mg_2SiO_4	MgSiO_3	SiO_2	Theory ^a
1	0.867	0.878	0.866	0.805	0.6
2	0.434	0.410	0.401	0.300	–

^aRosenfeld & Tarazona (1998).

using $\mathcal{O}_\theta = 2$, with the SiO_2 fit significantly further improved by excluding the $T = 6000$ K, $V/V_X = 0.8, 0.9$ and 1.0 points (white circles in Fig. 4). These points are at pressures below 15 GPa, where 6000 K is of less geophysical importance. Therefore, our preferred model for SiO_2 is $\mathcal{O}_\theta = 2$, which precludes extrapolation for this composition.

Thermodynamic properties at ambient pressure for the respective liquids are compared to previous experimental and theoretical estimates in Tables 3–6. Only partial molar experimental data for MgO liquid is available, and we mostly compare to previous theoretical estimates. Equation of state parameters differ slightly from those of Karki *et al.* (2006), because all the data are used in obtaining the equation of state fit. Values determined from $\mathcal{O}_\theta = 1$ and 2 are very similar; $\mathcal{O}_\theta = 1$ is sufficient to model the data. The added simulations at 2000 K for Mg_2SiO_4 and MgSiO_3 enable us to draw a direct comparison to experimental data collected at 1773 K. $\mathcal{O}_\theta = 1$ and 2 results are again very similar, and $\mathcal{O}_\theta = 1$ is sufficient to model the results. As with MgO, the 3000 K equation of state parameters parameters of SiO_2 also differ somewhat from those obtained by Karki *et al.* (2007). Notable discrepancies with α , C_V and C_P likely result from the large thermal extrapolation of experimental data. As noted

before, $\mathcal{O}_\theta = 1$ is not sufficient to represent the SiO_2 data; indeed $\mathcal{O}_\theta = 1$ and 2 results are rather different. Uncertainties in each thermodynamic property is estimated by repeated fitting to a Monte Carlo perturbation of the simulation data, constrained by its error estimates. As shown in Figs 1–4, $\mathcal{O}_\theta = 1$ fundamental relations yield αK_T , γ and C_V values similar to those obtained by (inconsistent) isochoric linear fits, and are well behaved upon extrapolation. In contrast, for $\mathcal{O}_\theta = 2$ these properties do not extrapolate well.

The ability of the liquid relation to capture the thermodynamics of the liquid–vapour transition is illustrated by extrapolating the Mg_2SiO_4 6000 K isotherm to very large volumes (Fig. 5). We ignore the thermal electronic contribution here, as it will vanish at such large volumes.

6.2 Solids

A third-order finite strain expansion is sufficient to fit the periclase simulations up to a compression ratio of $V/V_X = 0.45$, but we find that a fourth-order expansion is required to account for the points at higher pressures (Fig. 6). As found by Stixrude & Karki (2005), a third-order finite strain expansion is sufficient to fit the perovskite results, including the added data points at $V/V_X = 0.4$ (Fig. 7).

For periclase and perovskite, thermodynamic parameters at ambient pressure and reference temperature compare favourably with values from experiment and previous theoretical calculations (Tables 7 and 8). As previously concluded by Stixrude & Lithgow-Bertelloni (2005), we find the representation of $\gamma(V)$ using eq. (46)

Table 3. Thermodynamic properties of FPMD MgO liquid at 0 GPa, 3000 K.

	$\mathcal{O}_\theta = 1$	$\mathcal{O}_\theta = 2$	Previous estimates
V (cm ³ mol ⁻¹)	16.46(1)	16.46(1)	[16.50] ^a , [16.26] ^b , [16.03] ^{c,d} , <i>16.03</i> ^f
K_T (GPa)	35.3(1)	32.2(4)	[30.8(29)] ^a , [59.2] ^b
K_S (GPa)	45.5(4)	47.8(18)	<i>33 (1)</i> ^h
K'_T	4.65	4.92	[5.03(33)] ^a , [3.83] ^b
α (10 ⁻⁶ K ⁻¹)	100(1)	126(4)	204 ^f
S (Nk _B) ⁱ	10.51(5) ^j		<i>11.03</i> ^{d,e}
$C_V Nk_B$	3.6(2)	3.1(6)	[3.0(3)] ^a
$C_P Nk_B$	4.7(9)	4.7(12)	<i>5.19 (3)</i> ^g
γ	0.96(2)	1.28(9)	[0.95(7)] ^a , <i>1.25</i> ^{f,g,h}

Notes: Values of previous estimates shown in italics are extrapolated from lower temperature and/or measurements on other compositions, and values shown in [] are previous theoretical results.

^aKarki *et al.* (2006); ^bCohen & Gong (1994); ^cKarki *et al.* (2000); ^dAlfe (2005); ^eStixrude & Lithgow-Bertelloni (2005); ^fLange (1997); ^gStebbins *et al.* (1984); ^hAi & Lange (2008).

ⁱValue at melting temperature of 3070 K (Riley 1966; Zerr & Boehler 1994).

^jBased on periclase Gibbs free energy at an assumed melting point of 3070 K, 0 GPa (Riley 1966).

Table 4. Thermodynamic properties of FPMD Mg₂SiO₄ liquid at 0 GPa, 1773 K.

	$\mathcal{O}_\theta = 1$	$\mathcal{O}_\theta = 2$	Previous estimates
V (cm ³ mol ⁻¹)	51.9(1)	52.9(8)	<i>50.9</i> ^a
K_T (GPa)	33.4(2)	30.1(3)	<i>24.3 (1)</i> ^b
K_S (GPa)	36.6(3)	31.3(4)	<i>27 (3)</i> ^b
K'_T	5.15	5.23	<i>6.9</i> ^{d,i}
α (10 ⁻⁶ K ⁻¹)	86(5)	56(7)	<i>122 (7)</i> ^a
S (Nk _B) ^j	8.5(3) ^k		<i>8.10 (16)</i> ^{g,h}
$C_V Nk_B$	4.1(1)	3.7(6)	<i>3.7 (4)</i> ^{a,e}
$C_P Nk_B$	4.5(8)	3.8(15)	<i>3.9(4)</i> ^e , <i>5.1 (3)</i> ^f
γ	0.62(2)	0.42(4)	<i>0.56 (3)</i> ^{a,b,f} , <i>0.69 (4)</i> ^{a,b,e}

^aLange (1997); ^bAi & Lange (2008); ^cRivers & Carmichael (1987);

^dRigden *et al.* (1989); ^eTangeman *et al.* (2001); ^fStebbins *et al.* (1984);

^gNavrotsky *et al.* (1989); ^hStixrude & Karki (2005).

ⁱValue for CaMgSi₂O₆.

^jValue at melting temperature of 2163 K (Bowen & Andersen 1914).

^kBased on forsterite Gibbs free energy at an assumed melting point of 2163 K, 0 GPa (De Koker *et al.* 2008).

to give a superior comparison to previous theoretical estimates (insets in Figs 6 and 7).

7 APPLICATIONS

To illustrate the power of our method, we compute ambient pressure thermodynamic properties as well as high pressure melting curves and Hugoniot for MgO periclase and MgSiO₃ perovskite (orthoenstatite unshocked state), and the corresponding liquid phases. Our aim is to obtain a direct comparison of our simulation results to a broad range of low pressure measurements and high pressure shock loading data and make predictions of trends to expect where measurements have not yet been made.

Melting curves are obtained by finding the loci of pressure and temperature where solid and liquid Gibbs free energies correspond. As we use a reference melting temperature to constrain the liquid free energy from that of the solid, this approach is equivalent to integration of the Clapeyron equation, with integration done analytically rather than numerically.

For a given volume (V_h) or density (ρ_h), the theoretical Hugoniot state is given by the temperature (T_h) at which the pressure (P_h)

Table 5. Thermodynamic properties of FPMD MgSiO₃ liquid at 0 GPa, 1773 K.

	$\mathcal{O}_\theta = 1$	$\mathcal{O}_\theta = 2$	Previous estimates
V (cm ³ mol ⁻¹)	37.20(6)	38.02(8)	38.88 ^a
K_T (GPa)	27.3(2)	19.5(5)	16.81(7) ^b
K_S (GPa)	30.3(3)	21.0(5)	22(2) ^b
K'_T	5.71	7.17	<i>6.9</i> ^{c,h}
α (10 ⁻⁶ K ⁻¹)	102(3)	90(9)	84(4) ^a , 60 ^d
S (Nk _B) ⁱ	8.06(8) ^j		<i>7.62(6)</i> ^{e,f}
$C_V Nk_B$	4.2(1)	3.5(4)	4.2(2) ^g
$C_P Nk_B$	4.6(8)	3.7(13)	4.61(15) ^g
γ	0.60(2)	0.46(7)	0.37(14) ^{a,b,g}

^aLange (1997); ^bAi & Lange (2008); ^cRigden *et al.* (1989);

^dTomlinson *et al.* (1958); ^eRichet & Bottinga (1986); ^fStixrude & Lithgow-Bertelloni (2005); ^gStebbins *et al.* (1984).

^hValue for CaMgSi₂O₆.

ⁱValue at metastable congruent melting temperature of 1840 K (Bowen & Andersen 1914).

^jBased on perovskite Gibbs free energy at an assumed melting point of 2900 K, 25 GPa (and references therein Stixrude & Karki 2005).

and internal energy (E_h) satisfy the Rankine–Hugoniot relation,

$$(E_h - E_r) = -\frac{1}{2}(P_h + P_r)(V_h - V_r), \quad (57)$$

where E_r and V_r is, respectively, the internal energy and volume of the unshocked state defined by pressure P_r and temperature T_r .

Because internal energy and volume (density) are the natural thermodynamic variables along the Hugoniot, a first-order phase transition, such as univariant melting, occurs over a range of pressure–temperature conditions (Callen 1985). With increasing pressure, the Hugoniot intersects the melting curve, follows the melting curve for a finite interval of pressure along which the fraction of liquid increases, and then departs from the melting curve as the solid phase is exhausted. The liquid fraction along the melting portion of the Hugoniot is found by solving eq. (57) for a mechanical mixture of liquid and solid. Experiments may depart from this equilibrium picture due to kinetic effects including superheating (Luo 2003).

The sound velocity of the shock compressed phase can be measured in a shock loading experiment, with a large velocity decrease

Table 6. Thermodynamic properties of FPMD SiO₂ liquid at 0 GPa, 3000 K.

	$\mathcal{O}_\theta = 1$	$\mathcal{O}_\theta = 2$	Previous estimates
V (cm ³ mol ⁻¹)	27.2(2)	27.2(4)	[27.6] ^a , 28.7 ^b , 28.6 ^{c,b} , 26.9 ^d , 31 ^h
K_T (GPa)	12.2(5)	7.1(18)	[5.2(10)] ^a , 5.1 ^b
K_S (GPa)	12.2(8)	7.5(18)	10.6 (6) ⁱ
K'_T	6.3	17.1	[22.5(30)] ^a
α (10 ⁻⁶ K ⁻¹)	1.4(140)	121(12)	40.86 ^b , 12.3-123 ^j
S (Nk _B)		8.92(12) ^k	8.35 ^b , 8.26 ^{e,f,g}
$C_V Nk_B$	5.3(2)	5.2(6)	[5.0(4)] ^a
$C_P Nk_B$	5.3(9)	5.5(9)	3.4 ^b , 3.21 (3) ^e
γ	0.003(20)	0.18(4)	[0.2(1)] ^a

^aKarki *et al.* (2007); ^bHudon *et al.* (2002); ^cGaetani *et al.* (1998); ^dLange (1997); ^eStebbins *et al.* (1984); ^fRichet & Bottinga (1986); ^gStixrude & Lithgow-Bertelloni (2005); ^hBacon *et al.* (1960); ⁱAi & Lange (2008); ^jDingwell *et al.* (1993).

^kBased on stishovite Gibbs free energy at an assumed melting point of 3120 K, 14 GPa (Zhang *et al.* 1993; Shen & Lazor 1995).

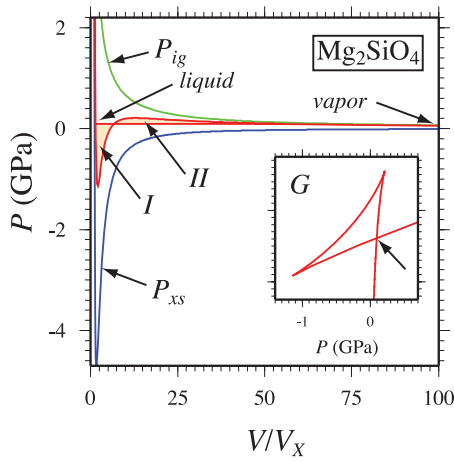


Figure 5. Thermodynamics of vapourization in Mg₂SiO₄ liquid. Eq. (16) also captures the thermodynamics of vapourization, as illustrated by extrapolation of the 6000 K isotherm in Mg₂SiO₄. The pressure of liquid–vapor coexistence (0.09 GPa; horizontal red line) is found from the triplication in G (arrow in inset), or equivalently from the Maxwell equal area construction (area I = area II). The resulting heat of vapourization (1130 kJ mol⁻¹) is comparable to the heat of vapourization of forsterite used in giant impact studies (Benz *et al.* 1989; Canup 2004).

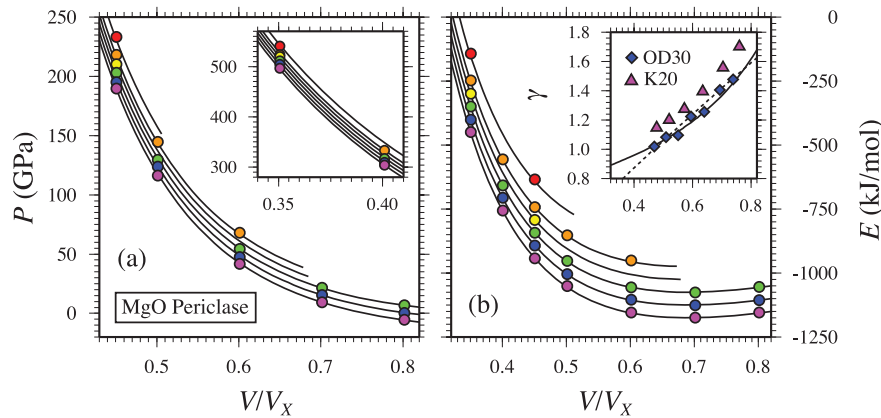


Figure 6. (a) Pressure (P), (b) internal energy (E) and (c) Grüneisen parameter (γ) of MgO periclase. Coloured circles show values from FPMD simulations at 2000 K (purple), 3000 K (blue), 4000 K (green), 5000 K (yellow), 6000 K (orange) and 8000 K (red). Black lines in (a) and (b) indicate the fit of eq. (35), with a fourth-order expansion in finite strain required to account for the points at $V/V_X = 0.35$ (left inset). Errorbars are smaller than the size of the symbols. Grüneisen parameter represented with eq. (46) (solid line) gives a superior fit to eq. (49) when compared to previous estimates (K20 – Karki *et al.* (2000), γ at 2000 K from lattice dynamics; OD30 – Oganov & Dorogokupets (2003), FPMD at 3000 K).

being a strong indication of melting. For a given phase, we compute v_P as

$$v_P = \sqrt{\frac{L}{\rho}}, \quad (58)$$

where L is the longitudinal modulus

$$L = K_S + 4/3\mu, \quad (59)$$

μ being the shear modulus. Because the deformation timescale in a shockwave experiment is long compared to the relaxation time of the liquid (Rigden *et al.* 1988), $\mu = 0$ and L reduces to

$$L = K_S. \quad (60)$$

K_S follows from eq. (8), and we obtain μ for the solid from experimental data using the model of Stixrude & Lithgow-Bertelloni (2005). Where liquid and solid coexist along the Hugoniot, we find the Voigt and Reuss bounds for L of the aggregate as (Watt *et al.* 1976)

$$L_R = \left(\sum x_i/L_i \right)^{-1} \leq L \leq \sum x_i L_i = L_V, \quad (61)$$

with the Hill average obtained as the arithmetic mean of L_R and L_V .

Our periclase melting curve differs only by a small degree from the previous first principles estimate of Alfe (2005) using FPMD simulation of direct phase coexistence in the LDA (Fig. 8). Both these curves are in general agreement with previous non-first principles theoretical estimates of the melting of periclase at high pressure (Cohen & Gong 1994; Vočadlo & Price 1996; Belonoshko & Dubrovinsky 1996; Cohen & Weitz 1998; Strachan *et al.* 2001), and are intermediate between the experimental determination of Zerr & Boehler (1994) and the compositional extrapolation of Zhang & Fei (2008). The slope remains positive over the entire pressure range considered.

The FPMD periclase Hugoniot agrees very well with the measured pressure–density Hugoniot (Marsh 1980; Vassiliou & Ahrens 1981; Svendsen & Ahrens 1987; Duffy & Ahrens 1995), as well as with the temperature measurements of Svendsen & Ahrens (1987). The periclase Hugoniot crosses the melting curve at $P = 375$ GPa, $T = 9580$ K, with the liquid phase periclase Hugoniot crossing the melting curve at $P = 470$ GPa, $T = 9870$ K. Complete shock

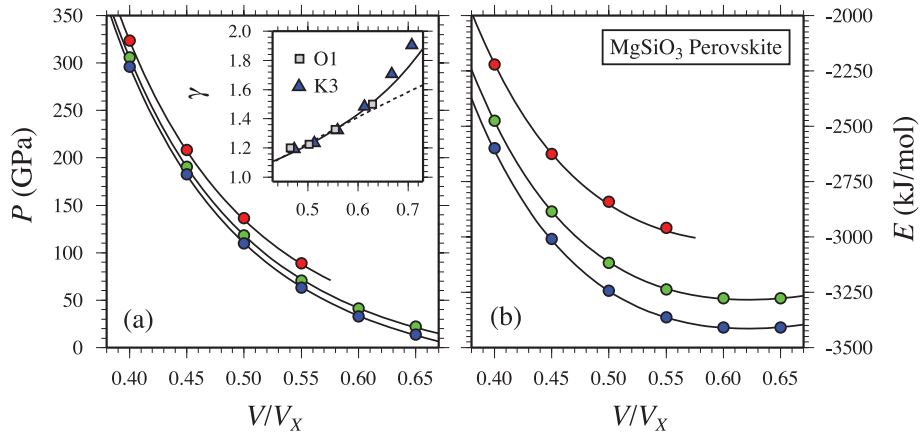


Figure 7. Same as Fig. 6, but for MgSiO₃ perovskite. Coloured circles show values from FPMD simulations at 3000 K (blue), 4000 K (green) and 6000 K (red). Black lines in (a) and (b) indicate the fit of eq. (35), with a third-order expansion in finite strain. K3 – Karki *et al.* (2000), γ at 3000 K from lattice dynamics; O1 – Oganov *et al.* (2001), FPMD at 1000 K.

Table 7. Thermodynamic properties of FPMD MgO periclase at 0 GPa, 2000 K.

	This study	Previous estimates
V (cm ³ mol ⁻¹)	12.22(1)	12.23 ^a
K_T (GPa)	108.3(8)	102 ^a
K_S (GPa)	126(1)	126 ^a
K'_T	4.89	4.97 ^a
K''_{TKT}	-6.57	-
$C_V Nk_B$	3.01(3)	2.98 ^a
$C_P Nk_B$	3.5(7)	3.69 ^a
α (10 ⁻⁶ K ⁻¹)	56.3(9)	68.7 ^a , 53 ^b , [64] ^c , [48] ^d
γ	1.49(3)	1.72 ^a , 1.47 ^e , [1.71] ^c , [1.69] ^d

^aStixrude & Lithgow-Bertelloni (2005); ^bTouloukian *et al.* (1977); ^cKarki *et al.* (2000); ^dOganov & Dorogokupets (2003); ^eIsaak *et al.* (1989).

Table 8. Thermodynamic properties of FPMD MgSiO₃ perovskite at 0 GPa, 2000 K.

	This study	Previous estimates
V (cm ³ mol ⁻¹)	25.87(1)	25.81 ^a , [26.26] ^b , [25.73] ^c
K_T (GPa)	204(5)	189.06 ^a , [181] ^b , [210.6] ^c
K_S (GPa)	231(11)	212.57 ^a
K'_T	4.14	4.96 ^a , [4.67] ^b , [4.49] ^c
α (10 ⁻⁶ K ⁻¹)	40(1)	40 ^a , [45.2] ^b , [37.3] ^c
$C_V Nk_B$	3.1(3)	2.97 ^a , [2.99] ^b
$C_P Nk_B$	3.5(9)	3.34 ^a , [3.46] ^b
γ	1.6(1)	1.57 ^a , [1.9] ^b , [1.51] ^c

^aStixrude & Lithgow-Bertelloni (2005); ^bKarki *et al.* (2000); ^cOganov *et al.* (2001).

melting is predicted to result in a ~ 0.14 g cm⁻³ density increase and a 2.2 km s⁻¹ sound velocity decrease along the Hugoniot.

The pressures at which we predict shock melting along the principal Hugoniot of periclase are very high, and beyond the current reach of shock wave experiments employing gas guns. However, shock melting can be achieved by using porous or pre-heated unshocked samples. We thus also calculate the shock melting interval for a number of pre-heated and porous starting materials (Tables 9 and 10).

Our perovskite melting curve (Fig. 9) is slightly different from the result of Stixrude & Karki (2005), as a result of the larger range of data used and the self-consistency imposed on the empirical correction for the overbinding of the LDA. The curve is somewhat colder than the measurements of Zerr & Boehler (1993) and Shen & Lazor (1995), though warmer than the experimental measurements of Knittle & Jeanloz (1989), Heinz & Jeanloz (1987) and Sweeney & Heinz (1998), as well as the result of Stixrude & Bukowinski (1990a). The Clapeyron slope remains positive over the entire pressure range considered.

The FPMD perovskite component of the enstatite principal Hugoniot compares well with the measured pressure–density Hugoniot (Akins *et al.* 2004) points at 149 and 170 GPa, but is notably warmer than the temperature measurements of Luo *et al.* (2004). The perovskite Hugoniot crosses the melting curve at $P = 150$ GPa, $T = 5190$ K, with the liquid phase Hugoniot crossing the melting curve at $P = 220$ GPa, $T = 5520$ K. Complete shock melting is predicted to result in a ~ 0.10 g cm⁻³ density increase and a 2.6 km s⁻¹ sound velocity decrease along the Hugoniot. Shock melting interval for a number of pre-heated and porous starting samples (orthoenstatite) are shown in Tables 11 and 12.

8 DISCUSSION

For a given order of expansion in the thermal variable (\mathcal{O}_θ), optimal values of m are remarkably similar for all four compositions considered. However, our results show that for $\mathcal{O}_\theta = 1$ these optimal values differ notably from the value of $m = 3/5$ expected theoretically for dense, simple liquids (Rosenfeld & Tarazona 1998). To see this, note that the internal energy expression derived from our liquid fundamental relation (eq. 26) is equivalent to the expression of (Rosenfeld & Tarazona 1998) for $\mathcal{O}_\theta = 1$ and $m = 3/5$

$$E_{\text{theory}}(V, T) = E_{\text{ig}}(T) + c_0(V) + c_1(V)T^{\frac{3}{5}}, \quad (62)$$

where $c_0(V)$ and $c_1(V)$ are functions only of volume. In addition, the assumption that E_{xs} is linear in $T^{\frac{3}{5}}$ breaks down in the case of SiO₂ which requires $\mathcal{O}_\theta = 2$ to accurately represent the FPMD results.

Our findings contrast those of previous semi-empirical MD studies of SiO₂, MgSiO₃ and Mg₂SiO₄ liquids (Saika-Voivod *et al.* 2001; Ghiorso *et al.* 2006; Martin *et al.* 2006), in which eq. (62) was assumed to hold for individual isochores, and highlight the

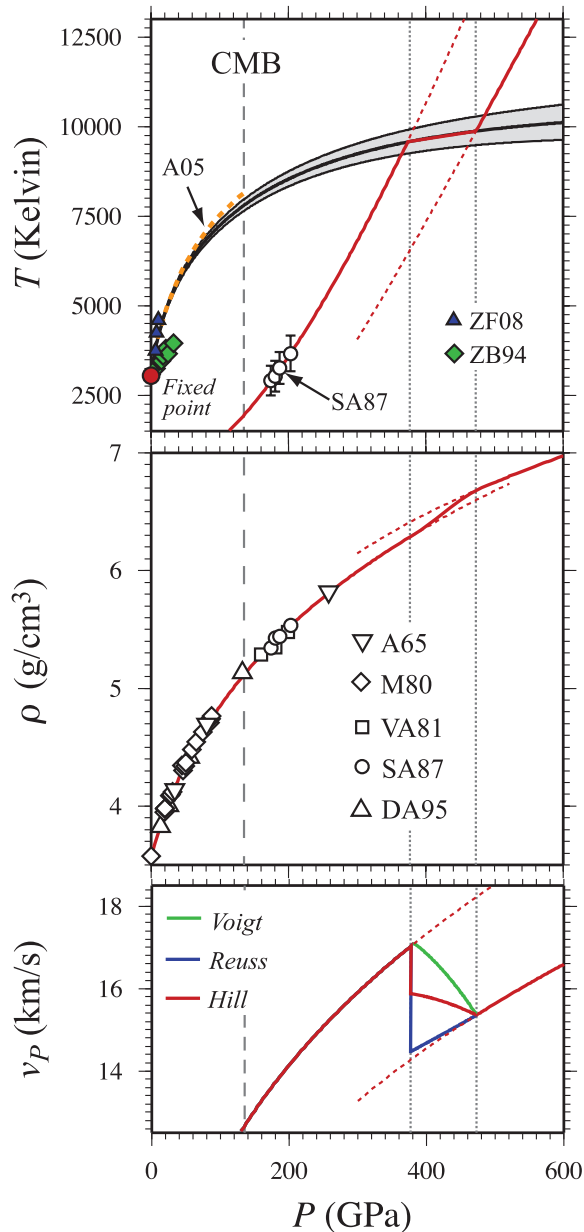


Figure 8. Shock melting of MgO periclaise. (top panel) FPMD melting curve of periclaise with uncertainty given by grey envelope. Melting temperature at the CMB is 7810 ± 160 K. Direct coexistence simulation using FPMD in the LDA of Alfe (2005) (A05; orange dotted line), and experimental measurements of Zhang & Fei (2008) (ZF08) and Zerr & Boehler (1994) (ZB94) shown for comparison. The solid Hugoniot crosses the melting curve at 375 GPa, 9580 K, and the liquid Hugoniot crosses at 470 GPa, 9870 K (faint dotted lines). In between these points the equilibrium Hugoniot follows the melting curve. Metastable Hugoniot sections are shown as broken lines. SA87 – shock temperature measurements of Svendsen & Ahrens (1987) (middle panel). Pressure–density Hugoniot, compared with experimental shock measurements of Al’tshuler *et al.* (1965) (A65), Marsh (1980) (M80), Vassiliou & Ahrens (1981) (VA81), Svendsen & Ahrens (1987) (SA87) and Duffy & Ahrens (1995) (DA95). Complete shock melting is predicted to result in a $\sim 0.14 \text{ g cm}^{-3}$ density increase along the Hugoniot, even though no density crossover is present along the melting curve. (bottom panel) Compressional wave velocity (v_P) of the liquid is 2.2 km s^{-1} slower than that of the solid calculated along the FPMD periclaise Hugoniot using experimental estimates of the shear modulus from Stixrude & Lithgow-Bertelloni (2005) (SLB05). Coloured lines in insipient melting section of Hugoniot represent the Voigt and Reuss bounds and the Hill average (Watt *et al.* 1976, see text).

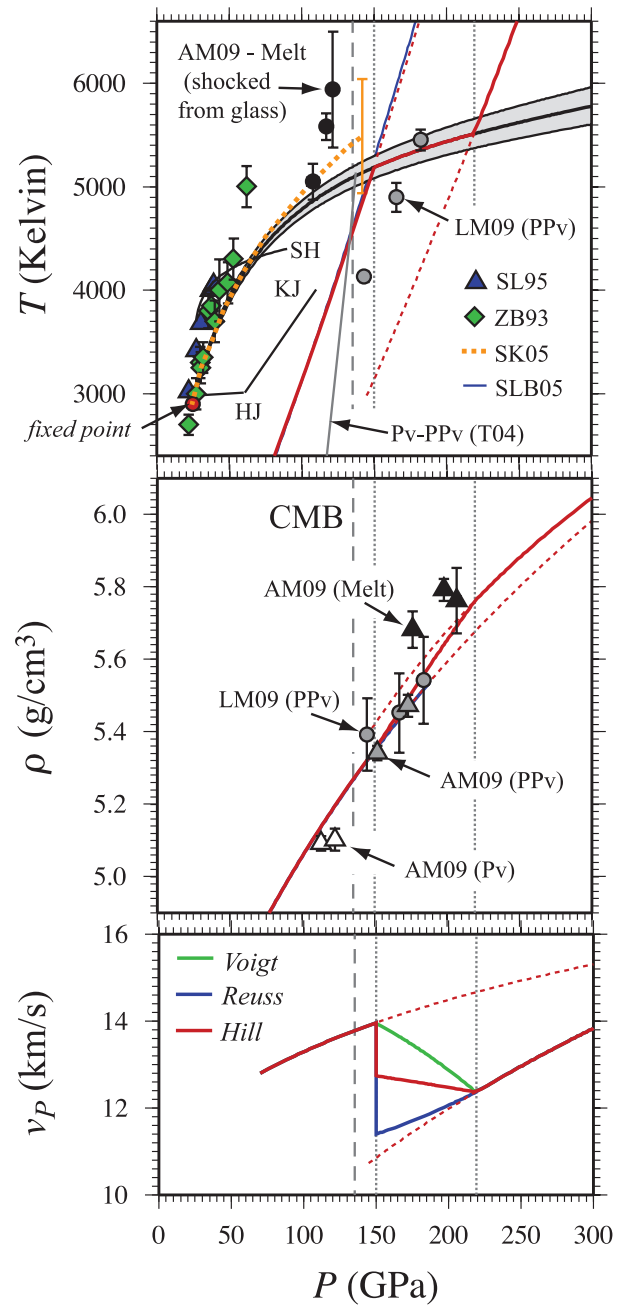


Figure 9. Same as Fig. 8, but for MgSiO_3 perovskite. (top panel) Melting temperature at the CMB is 5100 ± 100 K, which is within the uncertainty of the result of Stixrude & Karki (2005) (SK05; red dotted line). Experimental melting measurements are shown for Heinz & Jeanloz (1987) (HJ), Knittle & Jeanloz (1989) (KJ), Sweeney & Heinz (1998) (SH), Zerr & Boehler (1993) (ZB93), and Shen & Lazor (1995) (SL95), together with orthostate Hugoniot for perovskite calculated using the model of Stixrude & Lithgow-Bertelloni (2005). The solid Hugoniot crosses the melting curve at 150 GPa, 5190 K, and the liquid Hugoniot crosses at 220 GPa, 5520 K (faint dotted lines). LM09 and AM09 – shock temperature measurements for enstatite of Luo *et al.* (2004) and Akins *et al.* (2004), respectively, reassessed by Mosenfelder *et al.* (2009). T04 – Tsuchiya *et al.* (2004). (middle panel) Pressure–density Hugoniot, compared with experimental shock measurements. Complete shock melting is predicted to result in a $\sim 0.10 \text{ g cm}^{-3}$ density increase along the Hugoniot. (bottom panel) Compressional wave velocity (v_P) of the liquid is 2.6 km s^{-1} slower than that of the solid calculated along the FPMD perovskite Hugoniot using experimental estimates of the shear modulus Stixrude & Lithgow-Bertelloni (2005) (SLB05).

Table 9. Shock melting elastic properties of MgO periclase shocked from periclase pre-heated to T_0 at 0 GPa.

T_0 (K)	300		1000		1500		2000		2500	
	<i>init</i>	<i>compl</i>	<i>init</i>	<i>compl</i>	<i>init</i>	<i>compl</i>	<i>init</i>	<i>compl</i>	<i>init</i>	<i>compl</i>
P (GPa)	375	470	320	420	275	380	225	330	170	280
T (K)	9580	9870	9340	9730	9090	9590	8750	9390	8230	9110
ρ^{xtl} (g cm ⁻³)	6.28	6.72	6.00	6.50	5.75	6.31	5.44	6.05	5.06	5.78
ρ^{liq} (g cm ⁻³)	6.21	6.67	5.90	6.43	5.64	6.23	5.30	5.96	4.89	5.67
K_s^{xtl} (GPa)	1312	1588	1148	1444	1010	1327	854	1178	679	1026
K_s^{liq} (GPa)	1267	1566	1093	1409	951	1283	791	1125	615	966
v_p^{xtl} (km s ⁻¹) ^a	17.22	18.20	16.57	17.71	15.94	17.29	15.14	16.70	14.08	16.02
v_b^{xtl} (km s ⁻¹)	14.45	15.37	13.61	14.91	13.26	14.51	12.53	13.95	11.58	13.32
v_p^{liq} (km s ⁻¹)	14.29	15.33	13.82	14.80	12.99	14.35	12.21	13.74	11.22	13.06

Notes: *init* denotes the point along the Hugoniot where melting initiates, while *compl* denotes the point where melting is complete.

^aCalculated using experimental shear modulus from Stixrude & Lithgow-Bertelloni (2005).

Table 10. Shock melting elastic properties of MgO periclase shocked from porous periclase at 0 GPa, 300 K.

Porosity ρ_0 (g cm ⁻³)	0 per cent		5 per cent		10 per cent		20 per cent		30 per cent	
	<i>init</i>	<i>compl</i>	<i>init</i>	<i>compl</i>	<i>init</i>	<i>compl</i>	<i>init</i>	<i>compl</i>	<i>init</i>	<i>compl</i>
	3.58		3.40		3.22		2.86		2.51	
P (GPa)	375	470	315	410	260	350	175	255	115	180
T (K)	9580	9870	9320	9700	9000	9480	8290	8970	7500	8340
ρ^{xtl} (g cm ⁻³)	6.28	6.72	5.97	6.45	5.66	6.16	5.10	5.63	4.60	5.13
ρ^{liq} (g cm ⁻³)	6.21	6.67	5.88	6.38	5.54	6.07	4.93	5.51	4.38	4.97
K_s^{xtl} (GPa)	1312	1588	1132	1415	964	1238	695	948	496	711
K_s^{liq} (GPa)	1267	1566	1077	1377	903	1188	631	887	437	647
v_p^{xtl} (km s ⁻¹) ^a	17.22	18.19	16.50	17.61	15.72	16.94	14.18	15.64	12.64	14.29
v_b^{xtl} (km s ⁻¹)	14.45	15.37	13.77	14.81	13.05	14.18	11.68	12.98	10.34	11.77
v_p^{liq} (km s ⁻¹)	14.29	15.33	13.54	14.69	12.77	13.99	11.31	12.69	9.98	11.41

^aCalculated using experimental shear modulus from Stixrude & Lithgow-Bertelloni (2005).

Table 11. Shock melting elastic properties of MgSiO₃ perovskite, shocked from orthoenstatite pre-heated to T_0 at 0 GPa.

T_0 (K)	300		1000		1500	
	<i>init</i>	<i>compl</i>	<i>init</i>	<i>compl</i>	<i>init</i>	<i>compl</i>
P (GPa)	150	220	120	190	100	165
T (K)	5190	5520	4870	5390	4780	5270
ρ^{xtl} (g cm ⁻³)	5.35	6.33	5.10	5.65	4.92	5.47
ρ^{liq} (g cm ⁻³)	5.23	6.26	4.96	5.55	4.75	5.36
K_s^{xtl} (GPa)	696	1169	599	824	535	744
K_s^{liq} (GPa)	621	1183	507	772	431	678
v_p^{xtl} (km s ⁻¹) ^a	13.96	15.83	13.37	14.65	12.93	14.22
v_b^{xtl} (km s ⁻¹)	11.41	13.59	10.84	12.08	10.42	11.67
v_p^{liq} (km s ⁻¹)	10.90	13.75	10.12	11.79	9.53	11.25

Note: Orthoenstatite is metastable relative to protoenstatite above 1258 K (Atlas 1952).

^aCalculated using experimental shear modulus from Stixrude & Lithgow-Bertelloni (2005).

importance of determining the interatomic forces *in situ* from the electronic structure of the liquid.

In total, our formulation of the excess free energy requires the determination of eight free parameters for $\mathcal{O}_\theta = 1$, $\mathcal{O}_f = 3$: the relationships between the coefficients a_{00} , a_{10} , a_{20} , a_{30} , a_{01} , a_{11} , a_{21} and m (eq. 16), and the thermodynamic properties F_0 , V_0 , K_0 , K'_0 , S_0 , αK_{T_0} and $(d\alpha K_{T_0}/dV)_{T_0}$ are presented in the Appendix. While we have chosen to constrain parameters with the values of E and P computed from FPMD simulations, we note that experimental data could also be used to constrain the fundamental relation. Indeed, the

procedure for constraining parameters using dynamic compression experimental data would be very similar to what we have outlined here as the measured quantities on the Hugoniot are also E and P . Hugoniot data could be supplemented by precise measurements at low pressure, and thermochemical measurements of the heat capacity and entropy of the liquid at the ambient melting point might be used to constrain the value of m via

$$m = \frac{C_{V_{xs0}}}{S_{xs0}} + 1, \quad (63)$$

which follows directly from eq. (A10) and the condition $a_{02} = 0$ for $\mathcal{O}_\theta = 1$. We further note that the constraints on the value of m dictates that $S_{xs0} < 0$, that is, the total entropy of the liquid is less than that of the ideal gas. This order of fit appears to be sufficient for the silicate liquids we have studied to date with the exception of pure silica liquid. For pure silica liquid, $\mathcal{O}_\theta = 1$, $\mathcal{O}_f = 3$ may be adequate for many applications, but is not sufficient to represent our FPMD results over the entire volume–temperature range that we have explored. We have found that fits with $\mathcal{O}_\theta = 2$, which contain a much larger number of free parameters, appear to produce unphysical extrapolation outside of the fitted range, unlike those with $\mathcal{O}_\theta = 1$, which extrapolate physically to well beyond the fitted range.

The theoretical suitability of a Eulerian finite strain expansion for use with highly compressible materials such as silicate liquids has been questioned (Ghiorso *et al.* 2002; Ghiorso 2004; Hofmeister 1993). The two main concerns that have been cited, are firstly that analytical interatomic potentials derived from the Birch–Murnaghan equation of state predict non-physical effects for $K'_0 > 6$

Table 12. Shock melting elastic properties of MgSiO₃ perovskite, shocked from porous orthoenstatite at 0 GPa, 300 K.

Porosity $\rho_0(\text{g cm}^{-3})$	0 per cent 3.20		5 per cent 3.04		10 per cent 2.88		20 per cent 2.56		30 per cent 2.24	
	<i>init</i>	<i>compl</i>	<i>init</i>	<i>compl</i>	<i>init</i>	<i>compl</i>	<i>init</i>	<i>compl</i>	<i>init</i>	<i>compl</i>
$P(\text{GPa})$	150	220	125	190	105	160	75	115	50	80
$T(\text{K})$	5190	5520	5010	5390	4830	4250	4450	4930	3910	4530
$\rho^{xtl}(\text{g cm}^{-3})$	5.35	6.33	5.15	5.65	4.97	5.43	4.68	5.06	4.43	4.73
$\rho^{liq}(\text{g cm}^{-3})$	5.23	6.26	5.00	5.55	4.80	5.32	4.45	4.91	4.10	4.51
$K_s^{xtl}(\text{GPa})$	696	1169	616	824	551	728	454	583	375	470
$K_s^{liq}(\text{GPa})$	621	1183	526	772	450	659	335	488	238	354
$v_p^{xtl}(\text{km s}^{-1})^a$	13.96	15.83	13.46	14.65	13.03	14.14	12.33	13.27	11.65	12.45
$v_p^{xtl}(\text{km s}^{-1})$	11.41	13.59	10.94	12.08	10.53	11.58	9.85	10.74	9.21	9.97
$v_p^{liq}(\text{km s}^{-1})$	10.90	13.75	10.26	11.79	9.68	11.13	8.67	9.98	7.62	8.86

^aCalculated using experimental shear modulus from Stixrude & Lithgow-Bertelloni (2005).

(Hofmeister 1993), and secondly that the equation allows liquid bulk moduli to vanish at large volumes. Experimental and theoretical results for silicate liquids show K'_0 values to vary from around 5 to as high as 12 (Rigden *et al.* 1989; Lange 2003; Stixrude & Karki 2005; Karki *et al.* 2007; Lange 2007; Ai & Lange 2008; De Koker *et al.* 2008; Sun 2008). These high values reflect the ability of silicate liquids to access structural compression mechanisms not available to solids, such as changes in coordination (Williams & Jeanloz 1988) and ring statistics (Stixrude & Bukowinski 1990b), which enable liquids to become very compressible at high temperature and low density. The Hofmeister (1993) prediction only applies to simple ionic compounds, in which only the bond length is altered upon compression, and is therefore not relevant to silicate liquids. The second concern cited is, in fact, an asset of the finite strain expansion. When combined with an ideal gas term, as we have done, the relation shows a Van der Waals loop (Fig. 5), and thus also captures the thermodynamics of the liquid–vapour transition.

To the extent that the individual free energy contributions are separable, any thermodynamic property A which is a direct free energy derivative may be expressed as the sum of its individual contributions

$$A = A_{\text{ig}} + A_{\text{el}} + A_{\text{xs}}, \quad (64)$$

while other properties follow as rational combinations of the free energy derivatives, such as the Grüneisen parameter,

$$\gamma = (C_{V\text{ig}}\gamma_{\text{ig}} + C_{V\text{el}}\gamma_{\text{el}} + C_{V\text{xs}}\gamma_{\text{xs}})/(C_{V\text{ig}} + C_{V\text{el}} + C_{V\text{xs}}). \quad (65)$$

Values of the Grüneisen parameter obtained from the liquid fundamental relation therefore represent a weighted mean of the individual contributions. Because the thermo-electronic free energy contribution is considered negligible for the solid of interest here, the Grüneisen parameter calculated via the solid fundamental relation represents that arising due to changes in lattice vibrational frequencies with volume

$$\gamma_{\text{solid}} = -(\partial \ln \omega_{\text{D}}/\partial \ln V)_T, \quad (66)$$

where ω_{D} is the Debye frequency of the solid.

The relation for solids works well over the large range of pressure and temperature we consider, though the absence of a quantum correction requires caution in comparison with experimental equation of state data below the Debye temperature. The requirement of a fourth-order finite strain expansion for periclase is primarily due to the very large pressures attained in the smallest volume considered ($V/V_X = 0.35$). The relation requires only six (seven

for periclase) free parameters, and can therefore be extrapolated to higher temperatures and pressures with reasonable confidence.

The agreement with experiment of the theoretical periclase Hugoniot derived from our fundamental relation is very encouraging, and attests to the accuracy of FPMD at very high pressure and temperature, as well as to the utility of our method for modelling such information self-consistently. Agreement with pressure–density Hugoniot data for perovskite is good (Akins *et al.* 2004; Luo *et al.* 2004; Mosenfelder *et al.* 2009), but no comparison with shock temperature measurements is possible as existing measurements are believed to correspond to the post-perovskite phase (Luo *et al.* 2004; Mosenfelder *et al.* 2009). We note that a Hugoniot obtained using the thermodynamic model of Stixrude & Lithgow-Bertelloni (2005), which is constrained by a variety of non-dynamic experimental data is very similar to our FPMD Hugoniot. Furthermore, our melting curve is consistent with shock temperature measurements for MgSiO₃ glasses, believed to correspond to the molten phase (Luo *et al.* 2004; Mosenfelder *et al.* 2009). While the discrepancy between the density increase along the Hugoniot upon melting predicted by theory and that observed in experiment (Akins *et al.* 2004; Mosenfelder *et al.* 2009) is somewhat troubling, these three inferred liquid points are at pressures smaller than that at which we find the theoretical liquid Hugoniot to cross the melting curve, and are likely only partially molten.

The fact that the liquid Hugoniot is at a larger density than that of the solid in both periclase as well as perovskite should not be confused with a density crossover. The larger liquid Hugoniot density results simply due to thermal contraction as heat is absorbed during melting. Indeed, along the melting curves the densities of periclase and perovskite remain larger than that of the respective coexisting liquids, as reflected by the positive Clapeyron slopes. Our analyses show that computed Hugoniot and melting curves are insensitive to the choice of the reference melting point. An error in the assumed reference melting point translates into errors in computed high pressure Hugoniot and melting temperatures that are almost identical in magnitude. This is an important justification of our approach as low pressure melting properties are almost always more precisely known than the high pressure melting curves and Hugoniot that are our primary interest.

9 CONCLUSION

By extending the finite strain description of materials at high pressure of Birch (1952, 1978) to account for the thermal free energy contribution, we have constructed a thermodynamic description of

silicate liquids that is self-consistent and requires relatively few free parameters. Application of this relation to silicate liquids simulated by FPMD reveals that the effect of excited electronic states cannot be ignored in these materials at temperatures well above that of melting, and that existing theoretical predictions for the temperature dependence of the liquid free energy fail for silicate liquids at high temperature.

Of particular geophysical interest is the melting of mantle minerals at deep lower mantle pressures, most readily achieved in shock loading experiments. Shock melting may be identified by large changes in the temperature, discontinuities in density, and a marked decrease in the sound velocity of the shocked state measured along the Hugoniot. We are able to apply the thermodynamic description to obtain melting curves and Hugoniot loci for perovskite and periclase, compare to existing shock loading measurements and make quantitative predictions of each of the melting criteria. The agreement of the theoretical Hugoniot derived from our fundamental relation attests both to the accuracy of FPMD at very high pressure and temperature, and to the utility of our method for modelling such information self-consistently.

ACKNOWLEDGMENTS

This research was supported by the National Science Foundation under Grants EAR-0409074 and EAR-0409121, and in part by the European Commission under contract MRTN-CT-2006-035957. Computing facilities were provided by the Center for Computation and Technology at Louisiana State University and by the Center for Advanced Computing at the University of Michigan. We thank P. D. Asimow and an anonymous reviewer for helpful comments on the manuscript.

REFERENCES

Agee, C.B. & Walker, D., 1988. Static compression and olivine flotation in ultrabasic silicate liquid, *J. geophys. Res.*, **93**, 3437–3449.

Agee, C.B. & Walker, D., 1993. Olivine flotation in mantle melt, *Earth planet. Sci. Lett.*, **114**, 315–324.

Aguado, A. & Madden, P.A., 2005. New insights into the melting behaviour of MgO from molecular dynamics simulations: the importance of pre-melting effects, *Phys. Rev. Lett.*, **94**, 068501.

Ai, Y. & Lange, R.A., 2008. New acoustic velocity measurements on CaO-MgO-Al₂O₃-SiO₂ liquids: Reevaluation of the volume and compressibility of CaMgSi₂O₆-CaAl₂Si₂O₈ liquids to 25 GPa, *J. geophys. Res.*, **113**, B04203, doi:10.1029/2007JB005010.

Akins, J.A., Luo, S.N., Asimow, P.D. & Ahrens, T.J., 2004. Shock-induced melting of MgSiO₃ perovskite and implications for melts in Earth's lowermost mantle, *Geophys. Res. Lett.*, **31**, L14612.

Alfe, D., 2005. Melting curve of MgO from first-principles simulations, *Phys. Rev. Lett.*, **94**, 235701.

Allen, M.P. & Tildesley, D.J., 1987. *Computer Simulation of Liquids*, 1st edn, Oxford University Press, Oxford.

Al'tshuler, L.V., Trunin, R.F. & Simakov, G.V., 1965. Shock wave compression of periclase and quartz and the composition of the Earth's lower mantle, *Fizika zemli*, **10**, 1–6.

Anderson, O.L., 1995. *Equations of State of Solids for Geophysics and Ceramic Science*, Oxford University Press, New York.

Asimow, P.D., Hirschmann, M.M., Ghiorso, M.S., O'Hara, M.J. & Stolper, E.M., 1995. The effect of pressure-induced solid-solid transitions on decompression melting of the mantle, *Geochim. Cosmochim. Acta*, **59**(21), 4489–4506.

Atlas, L., 1952. The polymorphism of MgSiO₃ and solid-state equilibria of the system MgSiO₃ – CaMgSi₂ O₆, *J. Geol.*, **60**, 125–147.

Bacon, J.F., Hasapis, A.A. & Wholley, J.W., 1960. Viscosity and density of molten silica and high silica content glasses, *Phys. Chem. Glass.*, **1**, 90–98.

Belonoshko, A.B. & Dubrovinsky, L.S., 1996. Molecular dynamics of NaCl (B1 and B2) and MgO (B1) melting: two-phase simulation, *Am. Mineral.*, **81**, 303–316.

Belonoshko, A.B. & Saxena, S.K., 1992. A unified equation of state for fluids of C – H – O – N – S – Ar composition and their mixtures up to very high temperatures and pressures, *Geochim. Cosmochim. Acta*, **56**, 3611–3626.

Benz, W., Cameron, A.G.W. & Melosh, H.J., 1989. The origin of the moon and the single-impact hypothesis III, *Icarus*, **81**, 113–131.

Birch, F., 1952. Elasticity and constitution of the Earth's interior, *J. geophys. Res.*, **57**(2), 227–286.

Birch, F., 1978. Finite strain isotherm and velocities for single-crystal and polycrystalline NaCl at high pressures and 300 K, *J. geophys. Res.*, **83**(B3), 1257–1268.

Bottinga, Y., 1985. On the isothermal compressibility of silicate liquids at high-pressure, *Earth planet. Sci. Lett.*, **74**, 350–360.

Bowen, N.L. & Andersen, O., 1914. The binary system MgO-SiO₂, *Am. J. Sci.*, **37**, 487–500.

Boyle, R., 1662. *New Experiments Physico-Mechanical, Touching the Spring and Weight of the Air, and its Effects*, H. Hall, Oxford.

Brodholt, J. & Wood, B., 1993. Simulations of the structure and thermodynamic properties of water at high pressures and temperatures, *J. geophys. Res.*, **98**(B1), 519–536.

Bukowski, M.S.T., 1977. Theoretical equation of state for the inner core, *Phys. Earth planet. Inter.*, **14**(4), 333–344.

Callen, H.B., 1985. *Thermodynamics and an Introduction to Thermostatistics*, 2nd edn, John Wiley & Sons, New York.

Canup, R.M., 2004. Simulations of a late lunar-forming impact, *Icarus*, **168**, 433–456.

Ceperley, D.M. & Alder, B.J., 1980. Ground-state of the electron-gas by a stochastic method, *Phys. Rev. Lett.*, **45**, 566–569.

Chandrasekhar, S., 1939. *An Introduction to the Study of Stellar Structure*, University of Chicago Press, Chicago.

Chen, G.Q., Ahrens, T.J. & Stolper, E.M., 2002. Shock-wave equation of state of molten and solid fayalite, *Phys. Earth planet. Inter.*, **134**, 35–52.

Clapeyron, B.P.E., 1834. Mémoire sur la puissance motrice de la chaleur, *Journal de l'école polytechnique Paris*, **14**, 153–190.

Cohen, R.E. & Gong, Z., 1994. Melting and melt structure of MgO at high pressures, *Phys. Rev. B*, **50**(17), 12 301–12 311.

Cohen, R.E. & Weitz, J.S., 1998. The melting curve and premelting of MgO, in *Properties of Earth and Planetary Materials at High Pressure and Temperature*, *Geophysical Monograph*, Vol. **101**, pp. 185–196, eds Manghnani, M.H. & Yagi, T., American Geophysical Union, Washington, DC.

Cohen, R., Gülseren, O. & Hemley, R., 2000. Accuracy of equation-of-state formulations, *Am. Mineral.*, **85**, 338–344.

Courtial, P., Ohtani, E. & Dingwell, D.B., 1997. High-temperature densities of some mantle melts, *Geochim. Cosmochim. Acta*, **61**(15), 3111–3119.

De Koker, N.P., Stixrude, L. & Karki, B.B., 2008. Thermodynamics, structure, dynamics, and freezing of Mg₂SiO₄ liquid at high pressure, *Geochim. Cosmochim. Acta*, **72**, 1427–1441, doi:10.1016/j.gca.2007.12.019.

Dingwell, D.B., Knoche, R. & Webb, S.L., 1993. A volume temperature relationship for liquid GeO₂ and some geophysically relevant derived parameters for network liquids, *Phys. Chem. Miner.*, **19**, 445–453.

Dorogokupets, P.I., 2000. Thermodynamic functions at zero pressure and their relation to equations of state of minerals, *Am. Mineral.*, **85**, 329–337.

Dubrovinsky, L.S. & Saxena, S.K., 1997. Thermal expansion of periclase (MgO) and tungsten (W) to melting temperatures, *Phys. Chem. Miner.*, **24**, 547–550.

Duffy, T.S. & Ahrens, T.J., 1995. Compressional sound velocity, equation of state, and constitutive response of shock-compressed magnesium oxide., *J. geophys. Res.*, **100**(B1), 529–542.

- Feynman, R.P., Metropolis, N. & Teller, E., 1949. Equations of state of elements based on the generalized Fermi-Thomas theory, *Phys. Rev.*, **75**, 1561–1572.
- Flyvberg, H. & Petersen, H.G., 1989. Error-estimates on averages of correlated data, *J. Chem. Phys.*, **91**, 461–466.
- Francis, G.P. & Payne, M.C., 1990. Finite basis set corrections to total energy pseudopotential calculations, *J. Phys.-Condens. Matter*, **2**(19), 4395–4404.
- Frenkel, D. & Smit, B., 1996. *Understanding Molecular Simulation: From Algorithms to Applications*, 1st edn, Academic Press, San Diego.
- Gaetani, G.A., Asimow, P.D. & Stolper, E.M., 1998. Determination of the partial molar volume of SiO₂ in silicate liquids at elevated pressures and temperatures: a new experimental approach, *Geochim. Cosmochim. Acta*, **62**(14), 2499–2508.
- Garnero, E.J. & Helmberger, D.V., 1995. A very slow basal layer underlying large-scale low-velocity anomalies in the lower mantle beneath the Pacific: evidence from core phases, *Phys. Earth planet. Inter.*, **91**, 161–176.
- Ghiorso, M.S., 2004. An equation of state for silicate melts. I. Formulation of a general model, *Am. J. Sci.*, **304**, 637–678.
- Ghiorso, M.S. & Sack, R.O., 1995. Chemical mass transfer in magmatic processes IV. A revised and internally consistent thermodynamic model for the interpolation and extrapolation of liquid-solid equilibria in magmatic systems at elevated temperatures and pressures., *Contrib. Mineral. Petrol.*, **119**, 197–212.
- Ghiorso, M.S., Hirschmann, M.M., Reiners, P.W. & Kress, V.C., 2002. The pMELTS: a revision of MELTS for improved calculation of phase relations and major element partitioning related to partial melting of the mantle to 3 GPa, *Geochem. Geophys. Geosyst.*, **3**(5), doi:10.1029/2001GC000217.
- Ghiorso, M.S., Nevins, D. & Spera, F.J., 2006. Molecular dynamics studies of MgSiO₃ liquid to 150 GPa: an equation of state (EOS), tracer diffusivities, and a detailed analysis of changes in atomic coordination statistics as a function of temperature and pressure, *EOS, Trans. Am. geophys. Un.*, **87**(52), Fall Meeting Supplement, Abstract MR43B–1079.
- Gomes Dacosta, P., Nielsen, O.H. & Kunc, K., 1986. Stress theorem in the determination of static equilibrium by the density functional method, *J. Phys. C-Solid State Phys.*, **19**(17), 3163–3172.
- Halbach, H. & Chatterjee, N.D., 1982. An empirical Redlich-Kwong-type equation of state for water to 1000 °C and 100 Kbar, *Contrib. Mineral. Petrol.*, **79**, 337–345.
- Heinz, D.L. & Jeanloz, R., 1987. Measurement of the melting curve of Mg_{0.9}Fe_{0.1}SiO₃ at lower mantle conditions and its geophysical implications, *J. geophys. Res.*, **92**(B11), 11 437–11 444.
- Hicks, D.G., Boehly, T.R., Eggert, J.H., Miller, J.E., Celliers, P.M. & Collins, G.W., 2006. Dissociation of liquid silica at high pressures and temperatures, *Phys. Rev. Lett.*, **97**, doi:10.1103/PhysRevLett.97.025502.
- Hofmeister, A.M., 1993. Interatomic potentials calculated from equations of state: limitation of finite strain to moderate K' , *Geophys. Res. Lett.*, **20**(7), 635–638.
- Hohenberg, P. & Kohn, W., 1964. Inhomogeneous electron gas, *Phys. Rev. B.*, **136**, B864.
- Holland, T. & Powell, R., 1991. A compensated-Redlich-Kwong (CORK) equation for volumes and fugacities of CO₂ and H₂O in the range 1 bar to 50 kbar and 100–1600 °C, *Contrib. Mineral. Petrol.*, **109**, 265–273.
- Hudon, P., Jung, I.-H. & Baker, D.R., 2002. Melting of β -quartz up to 2.0 GPa and thermodynamic optimization of the silica liquidus up to 6.0 GPa, *Phys. Earth planet. Inter.*, **130**, 159–174.
- Isaak, D.G., Anderson, O.L. & Goto, T., 1989. Measured elastic moduli of single-crystal MgO up to 1800 K, *Phys. Chem. Miner.*, **16**, 704–713.
- Jeanloz, R., 1989. Shock wave equation of state and finite strain theory, *J. geophys. Res.*, **94**(B5), 5873–5886.
- Karki, B.B., Wentzcovitch, R.M., De Gironcoli, S. & Baroni, S., 2000. High-pressure lattice dynamics and thermoelasticity of MgO, *Phys. Rev. B.*, **61**(13), 8793–8800.
- Karki, B.B., Wentzcovitch, R.M., de Gironcoli, S. & Baroni, S., 2000. Ab initio lattice dynamics of MgSiO₃ perovskite at high pressure, *Phys. Rev. B.*, **62**(22), 14750–14756.
- Karki, B.B., Stixrude, L. & Wentzcovitch, R.M., 2001. High-pressure elastic properties of major materials of Earth's mantle from first principles, *Rev. Geophys.*, **39**, 507–534.
- Karki, B.B., Bhattarai, D. & Stixrude, L., 2006. First principles calculations of the structural, dynamical and electronic properties of liquid MgO, *Phys. Rev. B.*, **73**, 174208.
- Karki, B.B., Bhattarai, D. & Stixrude, L., 2007. First-principles simulations of liquid silica: structural and dynamical behaviour at high pressure, *Physical Review B*, **76**, 104205.
- Kirkwood, J.G., 1933. Quantum statistics of almost classical assemblies, *Phys. Rev.*, **44**, 31–37.
- Knittle, E. & Jeanloz, R., 1989. Melting curve of (Mg, Fe)SiO₃ perovskite to 96 GPa, evidence for a structural transition in lower mantle melts, *Geophys. Res. Lett.*, **16**(5), 421–424.
- Knopoff, L. & Uffen, R.J., 1954. The densities of compounds at high pressures and the state of the Earth's interior, *J. geophys. Res.*, **59**, 471–484.
- Kohn, W. & Sham, L.J., 1965. Self-consistent equations including exchange and correlation effects, *Phys. Rev.*, **140**, 1133.
- Kresse, G. & Furthmüller, J., 1996. Efficiency of ab-initio total energy calculations for metals and semiconductors using a plane-wave basis set, *Computat. Mater. Sci.*, **6**, 15–50.
- Kresse, G. & Hafner, J., 1994. Norm-conserving and ultrasoft pseudopotentials for first-row and transition-elements, *J. Phys.-Condens. Matter*, **6**, 8245–8257.
- Lange, R.A., 1997. A revised model for the density and thermal expansivity of K₂O – Na₂O – CaO – MgO – Al₂O₃ – SiO₂ liquids from 700 to 1900 K: extension to crustal magmatic temperatures, *Contrib. Mineral. Petrol.*, **130**, 1–11.
- Lange, R.A., 2003. The fusion curve of albite revisited and the compressibility of NaAlSi₃O₈ liquid with pressure, *Am. Mineral.*, **88**, 109–120.
- Lange, R.A., 2007. The density and compressibility of KAlSi₃O₈ liquid to 6.5 GPa, *Am. Mineral.*, **92**, 114–123.
- Lange, R.A. & Carmichael, I.S.E., 1987. Densities of Na₂O – K₂O – CaO – MgO – FeO – Fe₂O₃ – Al₂O₃ – TiO₂ – SiO₂ liquids—new measurements and derived partial molar properties, *Geochim. Cosmochim. Acta*, **51**, 2931–2946.
- Lange, R.A. & Navrotsky, A., 1992. Heat capacities of Fe₂O₃-bearing silicate liquids, *Contrib. Mineral. Petrol.*, **110**, 311–320.
- Laudernet, Y., Clérouin, J. & Mazevet, S., 2004. Ab initio simulations of the electrical and optical properties of shock-compressed SiO₂, *Phys. Rev. B.*, **70**, 165108.
- Luo, S.-N., Ahrens, T.J., Çağın, T., Strachan, A., Goddard, III, W.A. & Swift, D.C., 2003. Maximum superheating and undercooling: systematics, molecular dynamics simulations, and dynamic experiments, *Phys. Rev. B.*, **68**(13), 134206.
- Luo, S.N., Akins, J.A., Ahrens, T.J. & Asimow, P.D., 2004. Shock-compressed MgSiO₃ glass, enstatite, olivine, and quartz: optical emission, temperatures, and melting, *J. geophys. Res.*, **109**, B05205.
- Lupis, C.H.P., 1983. *Chemical Thermodynamics of Materials*, Prentice-Hall Inc., New York.
- Marsh, S.P., 1980. *LASL Shock Hugoniot Data*, University of California Press, Berkeley, CA.
- Marshak, R.E. & Bethe, H.A., 1940. The generalized Thomas-Fermi method as applied to stars, *Astrophys. J.*, **91**, 239–243.
- Martin, B., Spera, F.J. & Nevins, D., 2006. Thermodynamic and structural properties of liquid Mg₂SiO₄ at high temperatures and pressure in the range 0–150 GPa from molecular dynamics simulation, *EOS, Trans. Am. geophys. Un.*, **87**(52), Fall Meeting Supplement, Abstract MR43B–1080.
- Matsui, M., 1989. Molecular dynamics study of the structural and thermodynamic properties of MgO crystal with quantum correction, *J. Chem. Phys.*, **91**, 489–494.
- Matsukage, K.N., Jing, Z. & Karato, S., 2005. Density of hydrous silicate melt at the conditions of Earth's deep upper mantle, *Nature*, **438**, 488–491.
- McKenzie, D. & Bickle, M.J., 1988. The volume and composition of melt generated by extension of the lithosphere, *J. Petrol.*, **29**(3), 625–679.
- McQuarrie, D.A., 1984. *Statistical Mechanics*, University Science Books, Sausalito, CA.
- Mermin, N.D., 1965. Thermal properties of inhomogeneous electron gas, *Phys. Rev.*, **137**, 1441.

- Miller, G.H., Stolper, E.M. & Ahrens, T.J., 1991a. The equation of state of a molten komatiite. 1. Shock wave compression to 36 GPa, *J. geophys. Res.*, **96**(B7), 11 849–11 864.
- Miller, G.H., Stolper, E.M. & Ahrens, T.J., 1991b. The equation of state of a molten komatiite. 2. Application to komatiite petrogenesis and the hadean mantle, *J. geophys. Res.*, **96**(B7), 11 849–11 864.
- More, R.M., Warren, K.H., Young, D.A. & Zimmerman, G.B., 1988. A new quotidian equation of state (QEOS) for hot dense matter, *Phys. Fluids*, **31**(10), 3059–3078.
- Mosenfelder, J.L., Asimow, P.D. & Ahrens, T.J., 2007. Thermodynamic properties of Mg₂SiO₄ liquid at ultra-high pressures from shock measurements to 200 GPa on forsterite and wadsleyite, *J. geophys. Res.*, **112**(B06208), doi:10.1029/2006JB004364.
- Mosenfelder, J.L., Asimow, P.D., Frost, D.J., Rubie, D.C. & Ahrens, T.J., 2009. The MgSiO₃ system at high pressure: Thermodynamic properties of perovskite, post-perovskite, and melt from global inversion of shock and static compression data, *J. geophys. Res.*, **114**, B01203, doi:10.1029/2008JB005900.
- Navrotsky, A., Ziegler, D., Oestrike, R. & Maniar, P., 1989. Calorimetry of silicate melts at 1773 K—measurement of enthalpies of fusion and of mixing in the systems diopside-anorthite-albite and anorthite-forsterite, *Contrib. Mineral. Petrol.*, **101**, 122–130.
- Nosé, S., 1984. A unified formulation of the constant temperature molecular dynamics methods, *J. Chem. Phys.*, **81**, 511–519.
- Oganov, A.R. & Dorogokupets, P.I., 2003. All-electron and pseudopotential study of MgO: equation of state, anharmonicity, and stability, *Phys. Rev. B*, **67**, doi:10.1103/PhysRevB.67.224110.
- Oganov, A.R., Brodholt, J.P. & Price, G.D., 2001. The elastic constants of MgSiO₃ perovskite at pressures and temperatures of the Earth's mantle., *Nature*, **411**, 934–937.
- Ohtani, E., 1988. Chemical stratification of the mantle formed by melting in the early stage of the terrestrial evolution, *Tectonophysics*, **154**, 201–210.
- Ohtani, E. & Sawamoto, H., 1987. Melting experiment on a model chondritic mantle composition at 25 GPa, *Geophys. Res. Lett.*, **14**(7), 733–736.
- Panero, W.R. & Stixrude, L., 2004. Hydrogen incorporation in stishovite at high pressure and symmetric hydrogen bonding in δ-AlOOH, *Earth planet. Sci. Lett.*, **221**, 421–431.
- Pavese, A., 2002. Pressure-volume-temperature equations of state: a comparative study based on numerical simulations, *Phys. Chem. Miner.*, **29**, 43–51.
- Phillips, A.C., 1994. *The Physics of Stars*, John Wiley & Sons, Chichester.
- Pitzer, K.S. & Sterner, S.M., 1994. Equations of state valid continuously from zero to extreme pressures for H₂O and CO₂, *J. Chem. Phys.*, **101**(4), 3111–3116.
- Redlich, O. & Kwong, J.N.S., 1949. On the thermodynamics of solutions. 5. An equation of state—fugacities of gaseous solutions., *Chemical Reviews*, **44**(1), 233–244.
- Revenaugh, J. & Meyer, R., 1997. Seismic evidence of partial melt within a possibly ubiquitous low-velocity layer at the base of the mantle, *Science*, **277**, 670–673.
- Revenaugh, J. & Sipkin, S.A., 1994. Seismic evidence for silicate melt atop the 410 km mantle discontinuity, *Nature*, **369**(6480), 474–476.
- Richet, P. & Bottinga, Y., 1986. Thermochemical properties of silicate glasses and liquids: a review, *Rev. Geophys.*, **24**(1), 1–25.
- Rigden, S.M., Ahrens, T.J. & Stolper, E.M., 1984. Densities of liquid silicates at high pressures, *Science*, **226**(4678), 1071–1074.
- Rigden, S.M., Ahrens, T.J. & Stolper, E.M., 1988. Shock compression of molten silicate: results for a model basaltic composition, *J. geophys. Res.*, **93**(B1), 367–382.
- Rigden, S.M., Ahrens, T.J. & Stolper, E.M., 1989. High-pressure equation of state of molten anorthite and diopside, *J. geophys. Res.*, **94**(B7), 9508–9522.
- Riley, B., 1966. The determination of melting points at temperatures above 2000° celsius, *Revue Internationale des hautes Temperatures et des Refractaires*, **3**(3), 327–336.
- Rivers, M.L. & Carmichael, I.S.E., 1987. Ultrasonic studies of silicate melts, *J. geophys. Res.*, **92**, 9247–9270.
- Rosenfeld, Y. & Tarazona, P., 1998. Density functional theory and the asymptotic high density expansion of the free energy of classical solids and fluids, *Mol. Phys.*, **95**(2), 141–150.
- Saika-Voivod, I., Sciortino, F. & Poole, P.H., 2001. Computer simulations of liquid silica: equation of state and liquid–liquid phase transition, *Phys. Rev. E*, **63**, doi:10.1103/PhysRevE.63.011202.
- Sakamaki, T., Suzuki, A. & Ohtani, E., 2006. Stability of hydrous melt at the base of the Earth's upper mantle, *Nature*, **439**, 192–194.
- Shen, G. & Lazor, P., 1995. Measurement of melting temperatures of some minerals under lower mantle pressures, *J. geophys. Res.*, **100**(B9), 17 699–17 713.
- Slater, J.C. & Krutter, H.M., 1935. Thomas-Fermi method for metals, *Phys. Rev.*, **47**, 559–568.
- Solomatov, V.S. & Stevenson, D.J., 1993. Nonfractional crystallization of a terrestrial magma ocean, *J. geophys. Res.*, **98**(E3), 5391–5406.
- Song, T.R.A., Helmberger, D.V. & Grand, S.P., 1994. Low-velocity zone atop the 410 km seismic discontinuity in the northwestern United States, *Nature*, **427**(6974), 530–533.
- Span, R. & Wagner, W., 1997. On the extrapolation behaviour of empirical equations of state, *Int. J. Thermophys.*, **18**(6), 1415–1443.
- Stebbins, J.F., Carmichael, I.S.E. & Moret, L.K., 1984. Heat-capacities and entropies of silicate liquids and glasses, *Contrib. Mineral. Petrol.*, **86**, 131–148.
- Stixrude, L. & Bukowinski, M.S.T., 1990a. Fundamental thermodynamic relations and silicate melting with implications for the constitution of the D'', *J. geophys. Res.*, **95**(B12), 19 311–19 325.
- Stixrude, L. & Bukowinski, M.S.T., 1990b. A novel topological compression mechanism in a covalent liquid, *Science*, **250**, 541–543.
- Stixrude, L. & Karki, B.B., 2005. Structure and freezing of MgSiO₃ liquid in the Earth's lower mantle, *Science*, **310**, 297–299.
- Stixrude, L. & Lithgow-Bertelloni, C., 2005. Thermodynamics of mantle minerals — I. Physical properties., *Geophys. J. Int.*, **162**, 610–632.
- Stolper, E.M., Walker, D., Hager, B.H. & Hays, J.F., 1981. Melt segregation from partially molten source regions—the importance of melt density and source region size, *J. geophys. Res.*, **86**, 6261–6271.
- Strachan, A., Çağın, T. & Goddard III, W.A., 2001. Reply to comment on 'phase diagram of MgO from density-functional theory and molecular-dynamics simulations', *Phys. Rev. B*, **63**, doi:10.1103/PhysRevB.63.096102.
- Sun, N., 2008. Magma in earth's lower mantle: first principle molecular dynamics simulations of silicate liquids, *PhD thesis*, University of Michigan.
- Suzuki, A. & Ohtani, E., 2003. Density of peridotite melts at high pressure, *Phys. Chem. Miner.*, **30**, 449–456.
- Svendsen, B. & Ahrens, T.J., 1987. Shock-induced temperatures of MgO, *Geophys. J. R. astr. Soc.*, **91**, 667–691.
- Sweeney, J.S. & Heinz, D.L., 1998. Laser-heating through a diamond-anvil cell: melting at high pressures, in *Properties of Earth and Planetary Materials at High Pressure and Temperature*, *Geophysical Monograph*, Vol. 101, pp. 197–213, eds Manghnani, M.H. & Yagi, T., American Geophysical Union, Washington, DC.
- Tangeman, J.A., Phillips, B.L., Navrotsky, A., Weber, J.K.R., Hixson, A.D. & Key, T.S., 2001. Vitreous forsterite (Mg₂SiO₄): synthesis, structure, and thermochemistry, *Geophys. Res. Lett.*, **28**, 2517–2520.
- Tomlinson, J.W., Heynes, M.S.R. & Bockris, J.O., 1958. The structure of liquid silicates. Part 2. Molar volumes and expansivities, *Trans. Faraday Soc.*, **54**, 1822–1833.
- Touloukian, Y.S., Kirby, R.K., Taylor, E.R. & Lee, T.Y.R., 1977. *Thermophysical Properties of Matter—The TPRC Data Series*, Vol. 13: Thermal Expansion—Nonmetallic Solids., IFI/Plenum, New York.
- Trave, A., Tangney, P., Scandolo, S., Pasquarello, A. & Car, R., 2002. Pressure-induced structural changes in liquid SiO₂ from ab initio simulations, *Phys. Rev. Lett.*, **89**(24), 245504.
- Tsuchiya, T., Tsuchiya, J., Umemoto, K. & Wentzcovitch, R.M., 2004. Phase transition in MgSiO₃ in Earth's lower mantle, *Earth planet. Sci. Lett.*, **224**, 241–248.
- van der Waals, J.D., 1873. *Over de Continuïteit van den Gas- en Vloeïstoestand*, A.W. Sijthoff, Leiden.

- Vassiliou, M.S. & Ahrens, T.J., 1981. Hugoniot equation of state of periclase to 200 GPa, *Geophys. Res. Lett.*, **8**(7), 729–732.
- Vočadlo, L. & Price, G.D., 1996. The melting of MgO - computer calculations via molecular dynamics, *Phys. Chem. Miner.*, **23**, 42–49.
- Wan, J.T.K., Duffy, T.S., Scandolo, S. & Car, R., 2007. First-principles study of density, viscosity, and diffusion coefficients of liquid MgSiO₃ at conditions of the Earth's deep mantle, *J. geophys. Res.*, **112**, B03208.
- Watt, J.P., Davies, G.F. & O'Connell, R.J., 1976. The elastic properties of composite materials, *Rev. Geophys. Space Phys.*, **14**(4), 541–563.
- Wigner, E., 1932. On the quantum correction for thermodynamic equilibrium, *Phys. Rev.*, **40**, 749–759.
- Williams, Q. & Garnero, E.J., 1996. Seismic evidence for partial melt at the base of Earth's mantle, *Science*, **273**, 1528–1530.
- Williams, Q. & Jeanloz, R., 1988. Spectroscopic evidence for pressure-induced coordination changes in silicate glasses and melts, *Science*, **239**, 902–905.
- Wolf, G.H. & Jeanloz, R., 1984. Lindemann melting law - anharmonic correction and test of its validity for minerals, *J. geophys. Res.*, **89**, 7821–7835.
- Young, D.A. & Corey, E.M., 1995. A new global equation of state model for hot, dense matter, *J. Appl. Phys.*, **78**(6), 3748–3755.
- Zerr, A. & Boehler, R., 1993. Melting of (Mg,Fe)SiO₃-perovskite to 625 Kilobars: Indication of a high melting temperature in the lower mantle, *Science*, **262**, 553–555.
- Zerr, A. & Boehler, R., 1994. Constraints on the melting temperature of the lower mantle from high-pressure experiments on MgO and magnesio-wüstite, *Nature*, **371**, 506–508.
- Zhang, L. & Fei, Y., 2008. Melting behaviour of (Mg,Fe)O solid solutions at high pressure, *Geophys. Res. Lett.*, **35**, doi:10.1029/2008GL034585.
- Zhang, J., Liebermann, R.C., Gasparik, T. & Herzberg, C.T., 1993. Melting and subsolidus relations of SiO₂ at 9–14 GPa, *J. geophys. Res.*, **98**(B11), 19 785–19 793.

APPENDIX A: COEFFICIENTS OF F_{xs} IN THE LIQUID FUNDAMENTAL RELATION

The excess free energy contribution to the liquid state fundamental relation is given by

$$F_{\text{xs}}(V, T) = \sum_{i=0} \sum_{j=0} \frac{a_{ij}}{i!j!} f^i \theta^j, \quad (\text{A1})$$

$$f = \frac{1}{n} \left[\left(\frac{V_0}{V} \right)^{\frac{n}{3}} - 1 \right], \quad (\text{A2})$$

$$\theta = \left[\left(\frac{T}{T_0} \right)^m - 1 \right]. \quad (\text{A3})$$

By the assumption that the individual free energy contributions can be separated, any excess thermodynamic property (A_{xs}) which is a direct free energy derivative (instead of following from reduction of derivatives, such as the Grüneisen parameter) is obtained from the total value (A) by removing the ideal gas and electronic terms

$$A_{\text{xs}} = A - A_{\text{ig}} - A_{\text{el}}. \quad (\text{A4})$$

The coefficients of the excess free energy expansion (a_{ij}) are directly related to the excess thermodynamic properties of the liquid at reference volume (V_0) and temperature (T_0) and follow from taking the appropriate derivatives and substituting f_0 and θ_0 . These relations are

$$a_{00} = F_{\text{xs}0}, \quad (\text{A5})$$

$$a_{10} = 3V_0 P_{\text{xs}0}, \quad (\text{A6})$$

$$a_{01} = -\frac{1}{m} T_0 S_{\text{xs}0}, \quad (\text{A7})$$

$$a_{20} = 9V_0 K_{T_{\text{xs}0}} - 3(n+3)V_0 P_{\text{xs}0}, \quad (\text{A8})$$

$$a_{11} = \frac{3}{m} V_0 T_0 (\alpha K_T)_{\text{xs}0}, \quad (\text{A9})$$

$$a_{02} = -\frac{1}{m^2} T_0 C_{V_{\text{xs}0}} + \frac{m-1}{m^2} T_0 S_{\text{xs}0}, \quad (\text{A10})$$

$$a_{30} = 27V_0 K_{T_{\text{xs}0}} (K'_{T_{\text{xs}0}} - (n+2)) + 3(n+3)(2n+3)V_0 P_{\text{xs}0}, \quad (\text{A11})$$

$$a_{21} = -\frac{9}{m} V_0^2 T_0 \left(\frac{\partial \alpha K_T}{\partial V} \right)_{T, \text{xs}0} - \frac{3(n+3)}{m} V_0 T_0 (\alpha K_T)_{\text{xs}0}, \quad (\text{A12})$$

$$a_{12} = \frac{3}{m^2} V_0 T_0^2 \left(\frac{\partial \alpha K_T}{\partial T} \right)_{V, \text{xs}0} - \frac{3(m-1)}{m^2} V_0 T_0 (\alpha K_T)_{\text{xs}0}, \quad (\text{A13})$$

$$a_{03} = \frac{(3m-2)}{m^3} T_0 C_{V_{\text{xs}0}} - \frac{1}{m^3} T_0^2 \left(\frac{\partial C_V}{\partial T} \right)_{V, \text{xs}0} - \frac{(m-1)(2m-1)}{m^3} T_0 S_{\text{xs}0}, \quad (\text{A14})$$

$$a_{40} = 81V_0^3 \left(\frac{\partial^2 K_T}{\partial V^2} \right)_{T, \text{xs}0} + 162(n+2)V_0^2 \left(\frac{\partial K_T}{\partial V} \right)_{T, \text{xs}0} + 9V_0(11n^2 + 36n + 27)K_{\text{xs}0} - 3V_0(n+3)(6n^2 + 15n + 9)P_{\text{xs}0}, \quad (\text{A15})$$

$$a_{31} = \frac{27}{m} V_0^3 T_0 \left(\frac{\partial^2 \alpha K_T}{\partial V^2} \right)_{T, \text{xs}0} + \frac{27(n+3)}{m} V_0^2 T_0 \left(\frac{\partial \alpha K_T}{\partial V} \right)_{T, \text{xs}0} - \frac{3(n+3)(2n+3)}{m} V_0 T_0 (\alpha K_T)_{\text{xs}0}, \quad (\text{A16})$$

$$a_{22} = \frac{-9}{m^2} V_0^2 T_0 \left(\frac{\partial^2 C_V}{\partial V^2} \right)_{T, \text{xs}0} - \frac{3(n+3)}{m^2} V_0 T_0 \left(\frac{\partial C_V}{\partial V} \right)_{T, \text{xs}0} + \frac{9(m-1)}{m^2} V_0^2 T_0 \left(\frac{\partial \alpha K_T}{\partial V} \right)_{T, \text{xs}0} + \frac{3(n+3)(m-1)}{m^2} V_0 T_0 (\alpha K_T)_{\text{xs}0}, \quad (\text{A17})$$

$$a_{13} = \frac{3}{m^3} V_0 T_0^3 \left(\frac{\partial^2 \alpha K_T}{\partial T^2} \right)_{V, \text{xs}0} - \frac{9(m-1)}{m^3} V_0 T_0^2 \left(\frac{\partial \alpha K_T}{\partial T} \right)_{V, \text{xs}0} + \frac{3(m-1)(2m-1)}{m^3} V_0 T_0 (\alpha K_T)_{\text{xs}0}, \quad (\text{A18})$$

$$a_{04} = \frac{-1}{m^4} T_0^3 \left(\frac{\partial^2 C_V}{\partial T^2} \right)_{V, \text{xs}0} + \frac{2(3m-2)}{m^4} T_0^2 \left(\frac{\partial C_V}{\partial T} \right)_{V, \text{xs}0} - \frac{(11m^2 - 12m + 3)}{m^4} T_0 C_{V_{\text{xs}0}} - \frac{(m-1)(6m^2 - 5m + 1)}{m^4} T_0 S_{\text{xs}0}. \quad (\text{A19})$$